UC San Diego

UC San Diego Electronic Theses and Dissertations

Title

Understanding mechanisms by which injectable biomaterials affect cardiac function post-myocardial infarction

Permalink

https://escholarship.org/uc/item/4wt589vz

Author

Rane, Aboli Anil

Publication Date

2012

Peer reviewed|Thesis/dissertation

UNIVERSITY OF CALIFORNIA, SAN DIEGO

UNDERSTANDING MECHANISMS BY WHICH INJECTABLE BIOMATERIALS AFFECT CARDIAC FUNCTION POST-MYOCARDIAL INFARCTION

A dissertation submitted in partial satisfaction of the requirements for

the degree Doctor of Philosophy

in

Bioengineering

by

Aboli Anil Rane

Committee in charge:

       Professor Karen L. Christman, Chair
       Professor Andrew McCulloch
       Professor Jeffrey Omens
       Professor Kirk Peterson
       Professor Shyni Varghese

2012

The dissertation of Aboli Anil Rane is approved, and it is acceptable in quality and form for publication on microfilm and electronically:

_____

_____

_____

_____
                                                                          Chair

University of California, San Diego

2012

DEDICATION

For my family and friends, who never stopped believing in me.

TABLE OF CONTENTS

LIST OF FIGURES

LIST OF TABLES

aspirations from the day I joined UCSD. Dr. Peterson has been critical in guiding the clinical direction and focus for my research. It is through collaboration with Dr. Peterson and his lab, that I have been able to develop imaging expertise. Finally, I would like to thank Dr. Shyni Varghese for all her polymer insight, which has been invaluable. It has been a pleasure to work with each of my committee members at UC San Diego and I greatly appreciate all of their support through the years.

I would also like to acknowledge all of the graduate students and post-doctoral researchers that have helped shape my research. Dr. Adam Wright has patiently and taught me everything that I know about optical mapping. Adam is a great teacher and is always willing to make time to answer questions. I would also like to thank Dr. Joyce Chuang who taught me how to do MRI and SPAMM tagging. In addition I would like to acknowledge Dr. Miriam Scadeng, Dr. Kun Lu and Timothy Salazar for their help with MRI imaging at the center for functional MRI at UCSD as well as Rex Moats, Susan Lee, Gevorg Karapetyan and Ira Harutyunyan at the Children's Hospital in Los Angeles for their MRI technical support. I am also thankful for surgical support from Nancy Dalton and Yusu Hu. I would also like to acknowledge Dr. Anthony Demaria and Oi Ling Kwan for providing echocardiography expertise and Dr. Nissi Varki and Kimberly McIntyre for their assistance with histopathological analysis.

During my time at UCSD I have had the pleasure of being the professional development chair for the bioengineering graduate society for 3 years, through which I have interacted with numerous faculty, staff and industry associates who have influenced my personal and professional development; Jan Lenington, Lisa Dieu, Dr. Shankar Subramaniam, Dr. John Watson, Dr. Walt Baxter and Bob Balderas. I would also like to thank Dr. Melissa Micou for taking me on as an NSF REU coordinator and allowing me to create and implement a graduate student mentor training program. I would also like to thank Dr. Mark Kamps for accepting me in to the HHMI med-to-grad program and for his continual support through my graduate career. Furthermore, I would like to acknowledge Dr. Tsimikas and Dr. Kirk Knowlton for shaping my clinical cardiology experience. This program has influenced my career goals and direction in more ways than one.

I would also like to especially thank the members of the Christman Lab, who are not only incredible colleagues but also become my family in San Diego. The work in this thesis would not have been possible without the dedicated effort of our animal surgeons- Pam Schup-Magoffin, Rebecca Braden and Diane Hu. I would also like to acknowledge the past and present members of this lab- Dr. Jennifer Singelyn, Dr. Jessica DeQuach, Dr. Airong Song, Dr. Greg Grover, Sonya-Seif Naraghi, Adam Young, Nikhil Rao, Todd Johnson, Sophia Suarez and Jean Wang for being such a big part of my life both professionally and personally.

The following chapters are, in part, reprints of the following publications:

Chapter 1, in part is a reprint of material that is published as: Rane AR, Christman KL. Biomaterials for the treatment of myocardial infarction a 5-year update. J Am Coll Cardiol, 2011; 58 (25): 2615-29

Chapter 1, in part, is in submission as: Rane AR, Watson J, Christman KL. Tissue engineering and applications for treatment of myocardial infarction.

Chapter 1, in part, is a reprint of material that is published as: Rane AR, Chuang JS, Shah A, Hu DP, Dalton ND, Gu Y, Peterson KL, Omens JH, Christman KL. Increased Infarct Wall Thickness by a Bio-inert Material is Insufficient to Prevent Negative Left Ventricular Remodeling after Myocardial Infarction. PLoS ONE, 2011; 6 (6): e21571.

Chapter 2, in part, is a reprint of material that is published as: Rane AR, Chuang JS, Shah A, Hu DP, Dalton ND, Gu Y, Peterson KL, Omens JH, Christman KL. Increased Infarct Wall Thickness by a Bio-inert Material is Insufficient to Prevent Negative Left Ventricular Remodeling after Myocardial Infarction. PLoS ONE, 2011; 6 (6): e21571.

Chapter 4, in full, is in submission as: Rane AR, Wright AT, Suarez SL, Zhang SX, Braden RL, Almutairi A, McCulloch AD, Christman KL. Hydrogel injection in myocardium results in a potential substrate for arrhythmias.

Chapter 5, in part, is in submission as: Rane AR, Watson J, Christman KL. Tissue engineering and applications for treatment of myocardial infarction.

The author of this dissertation is one of the primary authors or co-author on all publications.

<h1 style="text-align: center">VITA</h1>

EDUCATION

September 2012
Ph.D., Bioengineering
Department of Bioengineering
University of California, San Diego

June 2009
M.S., Bioengineering
Department of Bioengineering
University of California, San Diego

May 2007
B.S., Chemical Engineering
Department of Chemical and Biomolecular
Engineering
Cornell University

AWARDS AND HONORS

American Heart Association Women in Cardiology Trainee Award for Excellence
(2010)
National Science Foundation Graduate Research Fellowship (2009-2012)
UC San Diego Diversity Fellowship (2008-2009)
UC San Diego Howard Hughes Medical Institute Med-to-Grad Fellowship (2008-
2009)
UC San Diego Powell-McLeroy Fellowship (2007-2008)

SELECTED PUBLICATIONS

AA. Rane, KL. Christman, *Biomaterials for the treatment of myocardial infarction: A 5-year update*, Journal of the American College of Cardiology, 2011.

AA. Rane, JS. Chuang, A. Shah, DP. Hu, ND. Dalton, Y. Gu, KL. Peterson, JH. Omens, KL. Christman, *Increased infarct wall thickness by a bio-inert material is insufficient to prevent negative left ventricular remodeling after myocardial infarction*, PlosOne, 2011.

ABSTRACT OF THE DISSERTATION

UNDERSTANDING MECHANISMS BY WHICH INJECTABLE BIOMATERIALS AFFECT CARDIAC FUNCTION POST-MYOCARDIAL INFARCTION

by

Aboli Anil Rane

Doctor of Philosophy in Bioengineering

University of California, San Diego, 2012

Professor Karen L. Christman, Chair

Cardiovascular disease affects over 82 million Americans, of which myocardial infarction (MI) and subsequent heart failure (HF) patients are a major subset. As a result, the development of new therapies for the prevention of HF is a rising clinical need. Several injectable materials have been shown to preserve or improve cardiac function as well as prevent or slow LV remodeling post-MI. However, the mechanism by which these materials influence cardiac function is not fully understood.

The objective of this dissertation is to investigate whether it is the structural support, bioactivity and/or degradation of these biomaterials that leads

to the beneficial effects seen with injectable materials used for treatment of MI. Furthermore, the impact of intramyocardial injection of these biomaterials on cardiac electrophysiology is assessed. Herein, we examined how passive structural enhancement of the LV wall by a permanent increase in wall thickness affected cardiac function post-MI using a bio-inert, non-degradable synthetic poly(ethylene) glycol (PEG) polymer. Contrary to popular opinion, passive structural reinforcement alone was insufficient to prevent post-MI remodeling.

As the next step in understanding the mechanism of action of injectable materials, a bio-inert synthetic degradable PEG was injected into the infarct site. Injection of degradable material resulted in a decline in cardiac function and undesirable changes in LV geometry similar to that of the non-degradable PEG. Thus, establishing that the ability for cell adherence and protein absorption may play an influential role in the improvement or preservation of cardiac function.

While most degradable bioactive materials have improved cardiac function, there remain concerns that biomaterial injection may create a substrate for arrhythmia. Optical mapping was utilized to assess the effects of biomaterial injection and spread on cardiac electrophysiology. Injection of a bulk biomaterial in myocardium may create a substrate for arrhythmia by causing activation delays and local heterogeneities in electrophysiological parameters at the site of injection. Therefore, delivery or spread of a material into viable or border zone myocardium may have deleterious effects, establishing site of delivery as an important factor of biomaterial therapies for MI treatment.

This work provides the field of cardiac tissue engineering guidelines for the future design and delivery of biomaterials, and moreover imparts a deeper understanding of the properties of biomaterials necessary to prevent post-MI negative remodeling and subsequent HF.

CHAPTER ONE:

Introduction

1.1 Myocardial infarction and subsequent heart failure

With myocardial infarction (MI) as a major contributor to cardiovascular disease, the leading cause of death in the western world, there is a rising need for novel therapies for treatment of post-MI negative left ventricular (LV) remodeling. Coagulative necrosis following MI initiates a cascade of events characterized by myocyte necrosis and their eventual replacement by fibrotic scar tissue. Necrosis of the myocytes triggers an inflammatory response leading to activation of matrix metalloproteinases [1] that cause a breakdown of the extracellular matrix, which results in myocyte slippage and infarct expansion. At the same time fibroblast proliferation occurs, leading to deposition of collagen and the formation of scar tissue. Concurrent TGF-β1 mediated transformation of fibroblast to myofibroblasts leads to deposition of type I and III collagen and scar tissue formation [2]. Ventricular wall thinning and dilatation also occurs leading to an increase in wall stress, [2-4]. While LV remodeling post-MI can be beneficial at first, over time this compensatory mechanism can be maladaptive, ultimately leading to heart failure (HF) [2].

Currently, pharmacologics, total heart transplantation, and LV assist devices are the only widespread forms of remedy for HF. However many experimental tissue engineering approaches are emerging for the treatment of adaptive LV remodeling and subsequent HF after MI. For approximately two decades, cellular cardiomyoplasty has been explored as a potential therapy, and

there are numerous ongoing clinical trials with some Phase III studies just beginning. Cell injection has, however, been limited by very poor retention and survival. A large portion of the transplanted cells can leak out of the tissue due to low viscosity of the injection medium (culture media or saline) contributing to poor retention of the cells [5]. In addition, cell survival is limited due to the hostile infarct environment, possible immune rejection by the host, and lack of a suitable matrix for cell adherence [6]. However, over the last decade or so, biomaterial technologies have emerged and shown great promise as potential treatments for MI.

1.2 Biomaterial therapies

Initially, tissue engineering approaches were explored in the heart to combat previous findings by providing an appropriate biomimetic environment for the injected cells to increase both engraftment and survival; moreover, more recently, acellular scaffold approaches that encourage endogenous cell infiltration are being utilized. Traditionally, an epicardial patch-based approach was utilized to deliver cells to the epicardial surface of the heart, which requires an open chest surgical procedure for implantation. To develop a potentially minimally invasive method for delivery, *in situ* gelling materials with or without cells or growth factors have been pursued, with some of these materials being catheter deliverable [7,8].

Both cellular and acellular biomaterial approaches for cardiac tissue engineering (Figure 1.1) have shown improved cardiac function, reduced infarct scar and increased neovascularization in the infarction zone. With the promising results seen from such therapies, many have moved into large animals pre-clinical trials and we are beginning to see these therapies move toward human application. A summary of LV patch and injectable cardiac technologies can be found in Table 1.1.
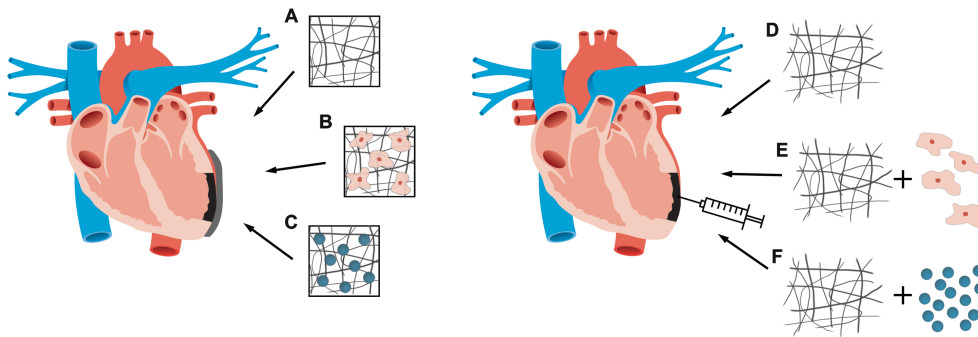
Figure 1.1: Biomaterial approaches to treatment of MI.
Cardiac tissue engineering consists of cardiac patches and injectable biomaterials. Cardiac patches and injectable materials can be either used as acellular scaffolds (A, D), or delivery vehicles for cells (B, E) and/or biological molecules (C, F). Reprinted with permission from [9].

Table 1.1: Cardiac tissue engineering therapies for MI

Material	Transplantation	Model	Ref
Cardiac Patch			
Gelatin	Alone	Rat	[10]
	w/ fetal CM		
Alginate	w/ fetal CM	Rat	[11]
Poly(glycolide)/poly(lactide)	w/ dermal fibroblasts	Mice	[12]
PTFE, PLA mesh, collagen Type I and matrigel	Alone	Rat	[13]
	w/ bone marrow-derived mesenchymal progenitor cells		
PTFE	Alone	Pig	[14]
Collagen Type I and matrigel	w/ neonatal CM, SkM	Rat	[15,16]
Collagen Type I	Alone	Rat, Human	[17-20]
	w/ ESCs, BMC, HUCBCs, hBMC CD133+, hMSC, hSkM		
	w/ VEGF		
Alginate and Matrigel	w/ SDF-1, IGF-1 and VEGF	Rat	[21]
	w/ neonatal CM + SDF-1, IGF-1 and VEGF		
Chitosan	Alone	Rabbit	[22]
	w/ FGF-2		
Fibrin	Alone	Pig	[23]
	w/ hESc derived ECs and hESC derived SMCs		
Polyurethane	w/SkM	Rat	[24,25]
Polyester urethane urea	Alone	Rat	[26]
Poly(glycolide-co-caprolactone)	Alone	Rat	[27]
	w//BMMNC		
Poly(lactide-co-€-caprolactone)	Alone	Rat	[28]
	w/ MSCs		
Decellularized myocardium/fibrin	w/mesenchymal progenitor cells	Rat	[29]
Small intestinal submucosa	w/ MSCs	Rabbit	[30]
Pericardium	w/ MSCs	Rat	[31]
Urinary bladder matrix	Alone	Pig	[14]
Injectable Biomaterials			
Fibrin	Alone	Mouse, Rat, Dog, Sheep	[32-38]
	w/ SkM, BMMNCs, BMCs, ACSs, MCSCs		
	w/ pleiotrophin plasmid, bFGF		
Alginate	Alone, RGD-modified, RGD+ YIGSR – modified, RGE - modified	Rat, Pig, Human	[8,39-46]
	w/VEGF, PDGF-BB, IGF-1, HGF		
	w/hMSCs		
	w/ polypyrrole		
Fibrin -Alginate	Alone	Pig	[47]
Chitosan	Alone	Rat	[48-50]
	w/ ESCs		
	w/ bFGF		
Gelatin	Alone	Rat, Dog	[51,52]
	w/bFGF		
Collagen	Alone	Rat, Pig	[53-55]
	w/ BMCs		
Matrigel	Alone	Mouse, Rat	[56,57]
	w/ ESCs, hESC derived CMs		
	w/ pro-survival factors		
Collagen Type I and Matrigel	Alone	Rat	[58]
	w/ neonatal CMs		
Small intestinal matrix	Alone	Mouse, Rat	[59,60]
Myocardial matrix	Alone	Rat, Pig	[61]
Pericardial matrix	Alone	Rat	[62]
Hyaluronic Acid	Alone	Rat, Sheep	[63,64]
Self-assembling peptides	Alone	Mouse, Rat, Pig	[65-68]
	w/ neonatal CMs, SkM + PDGF-BB, BMMNCs		
	w/ IGF-1, PDGF-BB, FGF-2		
Calcium Hydroxyapatite	Alone	Sheep	[69,70]

Table 1.1: Cardiac tissue engineering therapies for MI Continued

PEG based	Alone	Rat, Rabbit	71-77
	w/ BMSC, hESC + thymosin ß4		
	w/ VEGF, thymosin ß4, erythropoietin		
PNIPAAm based	Alone	Rat, Rabbit	78-82
	w/ BMMNCs, BMSC		
	w/ bFBF		

ASC – Adipose derived stem cell
bFGF – Basic fibroblast growth factor
BMC – Bone marrow cell
BMMNC – Bone marrow-derived mononuclear cell
BMSC – Bone marrow derived stem cell
CM – Cardiomyocyte
EC – Endothelial cell
ESC – Embryonic stem cell
FGF - Fibroblast growth factor
HGF - Hepatocyte growth factor
HUCBC – Human umbilical cord blood mononuclear cell
HUVEC – Human umbilical vein endothelial cell
IGF – Insulin-like growth factor
MCSC – Marrow-derived cardiac stem cell
MSC – Mesenchymal stem cell
PCL – Polycaprolactone
PDGF – Platelet-derived growth factor
PEG – Poly(ethylene glycol)
PNIPAAM - Poly(N-isopropylacrylamide)
PLA – Polylactic acid
PTFE – Polytetrafluoroethlyene
SDF - Stromal cell derived factor
SkM – Skeletal myoblast
VEGF – Vascular endothelial growth factor

1.3 Cardiac patches

Initially, cardiac patches involved the use of biomaterial scaffolds to enhance cell delivery and more recently have been used as an acellular therapy. It is thought that the microenvironment and architecture provided by such a scaffold can support cellular differentiation and organization, and prevent anoikis (cell death from detachment) [83]. Application of various biomaterials with a variety of cell types has shown an improvement in cardiac function in small animals. Nonetheless, one major drawback with this method remains the inability to generate patches with sizable thickness due to diffusion limitations [5,83]. In the last

five years, many different scaffolds have been examined *in vitro* for such applications [83].

Of the different materials used for the fabrication of cardiac patches in recent years, collagen, the predominant protein in the extracellular matrix, has been used extensively alone and with cells. Callegari et al., showed that application of a collagen sponge to a rat cryoinjury model immediately post-injury injury led to increased angiogenesis compared to the control, 15 and 60 days post-implantation of the patch [17]. Additionally, delivery of human bone marrow-derived CD133$^+$ cells (4 x 10^6 cells) with a collagen scaffold increased the number of vessels in a rat cryoinjury model, however there was no significant differentiation into cardiomyocytes [19]. Similarly, application of a human mesenchymal stem cell (MSC) (1 x 10^6 cells) seeded collagen scaffold immediately post-infarction resulted in a 30% increase in fractional shortening (FS) in the patch-treated group compared to the control in a rodent model [20]. Hamdi et al. compared intramyocardial delivery of cells to a cardiac patch-based approach. Human skeletal myoblasts ($5x10^6$ cells), control medium, a bilayer myoblast cell sheet, or a myoblast seeded collagen sponge was injected or implanted at the site of infarction, 4 weeks post-MI. Animals that received the cell sheet and seeded cell scaffold showed significant improvement in ejection fraction (EF) and increased vessel density compared to the control, one month post-implantation [84]. In the Myocardial Assistance by Grafting a New Bioartificial Upgraded Myocardium (MAGNUM) phase 1 clinical trial, a collagen type I patch

seeded with bone marrow cells was applied on 10 patients that had coronary artery bypass graft and intrainfarct implantation of autologous bone marrow cells. Both the combined approach of cell injection and a cardiac patch as well as the cell injection alone showed an improvement in EF at a 10 ± 3.5 months follow-up compared the baseline measurement 1 week before coronary artery bypass. However, LV ED volume and scar thickness were improved in the patients that received a cell-seeded collagen patch combined with cellular injection compared to those receiving the intrainfarct cell injection alone [18]. Similarly, an improvement in EF was seen in a mouse MI model upon application of a collagen patch seeded with human umbilical cord mononuclear cells (5×10^6 cells) along with an injection of the same cell type (5×10^6 cells) or by the injection of the cells alone 45 days post-treatment when compared to the baseline, while deterioration of function was seen in the scaffold only and control groups.

Giraud et al. showed improvement in FS, 4 weeks post-treatment, using a combination patch of collagen type I, Matrigel and rat skeletal muscle cells adhered on the surface of the heart with fibrin glue, 2 weeks post-MI in a rodent model [85]. Similarly, Dvir et al. constructed a patch by seeding an alginate scaffold with neonatal cardiomyocytes (7×10^7 cells/cm^3) in Matrigel and pro-survival and angiogenic factors. The patch was cultured in the rat omentum for 7 days to promote maturation of vasculature and then transplanted into infarcted rats one week post-infarction. At 28 days post-implantation this pre-vascularized patch showed structural and electrical integration with the host myocardium as

well as preservation of FS and fractional area change [21]. Another bio-derived scaffold, fibrin, has also been seeded with human embryonic stem cell derived endothelial cells (2 x 10^6 cells) and smooth muscle cells (2 x 10^6 cells). Implantation in a porcine model immediately post-MI resulted in improved EF at 7 days and persisted till 4 weeks [23].

A recent development has been the use of decellularized organs for the creation of cardiac patches representing the complex milieu of the native extracellular matrix. Ott et al. first demonstrated the ability to decellularize the myocardium [86]. Godier-Furnemont et al. seeded human MSCs (1 x 10^6 cells) in fibrin on a decellularized human myocardial sheet. Implantation of the scaffold preserved FS and LV diameter as well as an enhanced vascular network by secretion of paracrine factors and migration of the MSCs in the damaged myocardium 4 weeks post-treatment in a rat MI model [29]. Similarly, decellularized small intestinal submucosa (SIS) itself or seeded with MSCs in a rabbit MI model 4 weeks post-treatment led to an improvement in LV ES and ED diameters and EF compared to the control. Furthermore, animals treated with the MSC-seeded SIS had a significantly greater improvement in EF compared to the animals treated with the SIS alone [30]. Likewise, a patch made with a sliced decellularized pericardial tissue scaffold inserted with multilayered MSCs was used to replace the infarcted myocardium in a rodent model, and resulted in greater FS, higher LV ES pressure, and lower LV ED pressure when compared to the control [31]. Though there are only limited studies using an organ derived

scaffold in the heart to date, this will likely increase given the rapidly expanding use of decellularized scaffolds in tissue engineering.

Along with biologically derived materials, a number of synthetic materials have been explored. Fujimoto et al. showed that application of an elastic biodegradable polyester urethane urea scaffold over a 2 week rodent infarct led to an increase in regional fractional area change, wall thickness, and capillary density compared to the control MI group 8 weeks post-implantation [26]. Siepe et al. generated a scaffold by seeding rat skeletal myoblasts on highly porous polyurethane scaffold. After implantation 2 weeks post-MI in a rat model, there was evidence that both the muscle grafts and the injection of skeletal myoblasts alone led to improved contractile function and increased EF 4 weeks post-implantation, compared to the acellular scaffold group and the control [24,25]. In a follow-up long-term study, prevention of heart failure was seen up to 9 months, however this diminished by 12 months, indicating such a therapeutic approach may have transient benefit [87]. Piao et al. implanted biodegradable poly(glycolide-co-caprolactone) with or without bone marrow-derived mononuclear cells 7 days post-infarction in a rat. Four weeks post-implantation there was improved FS, LV ED pressure, and LV ED and ES diameters in both scaffold groups compared to the sham-operated group [27]. Another study compared the effectiveness of direct cell injection versus a cardiac patch based approach. MSCs (1×10^6 cells) were directly transplanted into the border of a cryoinjury infarct or seeded onto poly(lactide-co-€-caprolactone) and implanted over the infarct area ten days post-

MI. EF increased by 23% and the infarct area decreased by 29% in the polymer + MSC group compared to saline and the acellular scaffold, 4 weeks post-treatment. Similar results were seen in the MSC only group [28].

1.4 Injectable biomaterials

Over the last five years, there has been extensive growth in the field of injectable biomaterials for treating MI. These materials have been injected alone or used as delivery vehicles for cells and/or biological moieties. Injectable materials have shown positive results such as improvement in cardiac function, reduction of infarct size and increase in neovascularization. It is now well established that delivery of cells in a biomaterial can improve cellular retention and viability. Given the promise of this approach, materials have advanced to large animal pre-clinical models and even early clinical trial stage [46]. Most notably, materials such as alginate and myocardial matrix have gelation properties that facilitate percutaneous delivery into the myocardium [88-90], alleviating the need for invasive procedures required for the application of LV restraints and cardiac patches.

Proof-of-concept for the ability of injectable biomaterials alone to preserve cardiac function post-MI and to improve cell transplant survival was first demonstrated with fibrin in a rat ischemia-reperfusion model [91,92]. This initial study utilized skeletal myoblasts, and these results have since been confirmed with a variety of cell types such as bone marrow cells [33], marrow-derived cardiac

stem cells [35] and adipose-derived stem cells [34,36]. In some studies fibrin alone caused improvement in function similar to that of injection of fibrin with cells, while in others cases an enhancement of cardiac function was seen by adding cells to the biomaterial. The reason for the discrepancy is unclear, but it could be due to the difference in the rat MI models used. Injection of cells may provide additional value compared to acellular injection; however, to date many studies show similar improvements in cardiac function with a biomaterial alone. Basic fibroblast growth factor (bFGF) in fibrin [38], hepatocyte growth factor in a pegylated fibrin [32], and transforming growth factor ß-1 in poly (lactic-co-glycolic acid) microspheres and bone marrow mononuclear cells in a fibrin gel [37] have also been explored for treatment of MI. In a pig model, direct microinjections of a fibrin-alginate composite in the infarct, one week post-MI preserved wall thickness and decreased infarct expansion 7 days post-injection [47]. One potential concern with fibrin, however, is the two-component system made of fibrinogen and thrombin, making minimally invasive delivery a challenge.

The pivotal work done in 2005 by Leor et al. has paved the way for the use of alginate as a scaffold for myocardial tissue engineering for injection alone or as a scaffold for growth factor or cell delivery [93]. In the last 5 years, major progress has been made with this seaweed-derived polysaccharide. Landa et al., showed that injection of alginate at 1 week in a rat MI resulted in increased scar thickness and improved LV ES and ED area compared to saline two months post-injection. These results were similar or superior to injection of neonatal

cardiomyocytes. At 6 weeks post-injection the biomaterial was degraded, thus the increase in wall thickness was potentially due to infiltrating myofibroblasts. In addition, alginate was injected in late infarcts (8 weeks) and assessed two months later, showing a similar increase in scar thickness and improvement in systolic and diastolic function [44]. Delivery of vascular endothelial growth factor (VEGF) as well as sequential delivery of VEGF followed by platelet derived growth factor [41] or insulin-like growth factor and hepatocyte growth factor [40] in alginate showed improvement in LV remodeling compared to the biomaterial alone and the control 4 weeks post-injection in a rat MI . The effects of surface modification of alginate was also studied by injection of alginate modified with RGD or unmodified alginate 5 weeks post-MI into a rat LV aneurysm model. Improvement in LV ES and ED diameter as well increased arteriole presence was observed in both groups compared to saline [39]. Injection of RGD-modified alginate microbeads with and without human MSCs in a one week rodent MI led to improvement in FS and preservation of wall thickness and LV internal diameter 10 weeks post-injection [42]. Contrary to these studies, Tsur-Gang et al. showed that modification of alginate by RGD and YIGSR or the control RGE peptide was not as effective as unmodified alginate in improvement of scar thickness and FS, 60 days post injection into a one-week rat infarct. It is hypothesized that this discrepancy could be due to alteration in viscosity upon addition of the peptides that led to changes in distribution of the material and reduced coverage of the infarct [43]. In addition, alginate has been blended with the electroactive polymer polypyrrole showing an

increase in arteriole density 5 weeks post-treatment compared to alginate alone and saline upon injection in a rat MI [45]. Leor et al. carried out pre-clinical work with alginate in a swine MI model showing that intracoronary injection of alginate led to prevention and reversal of negative LV remodeling. Saline-injected animals had an increase in LV ED and ES area as well as LV mass, however injection of 2 ml or 4 ml of alginate led to preservation or improvement in LV area, but not FS. The 2 ml injection increased scar thickness by 53% compared to saline, possibly due to myofibroblasts migration and deposition of collagen [8]. These results have recently led to a "first in man" safety and feasibility study of intracoronary injection of alginate in acute MI patients [46].

As with cardiac patches, the use of decellularization as a technique for preparation of injectable materials is growing at a rapid pace. Injection of decellularized SIS extracellular matrix into an ischemia-reperfusion rat model promoted cell migration (c-kit$^+$ cells, myofibroblasts and macrophages) and improvement in cardiac function in terms of EF and stroke volume compared to the saline control [60]. Okada et al. injected two forms of SIS-derived gels immediately post-MI in a murine model. One form, SIS-B, improved LV ES area and fractional area change compared to SIS-C and the control at 2 weeks post-treatment but not at 6 weeks. However, SIS-B reduced infarct size and increased capillary density compared to SIS-C and the control only at 6 weeks. These differences are potentially attributed to increased bFGF content and greater stiffness of the gel [59]. While general extracellular matrix components among

tissues are similar, heterogeneity exists in the combination of proteins and proteoglycans [94]. Given the complex extracellular structure of the heart, the injection of a cardiac specific matrix may be better suited for treating the myocardium.   Singelyn et al. developed an injectable hydrogel form of decellularized porcine ventricular tissue, which was first tested in healthy myocardium [61]. More recently, it was shown that this material preserved cardiac function in a rat MI model and is compatible with percutaneous transendocardial delivery in pigs [89]. Seif-Naraghi et al., created and injected an acellular pericardial matrix gel into healthy rodent myocardium as proof-of-concept for a potentially autologous therapy for MI [62] and has also demonstrated that this material can be formed from samples from a variety of human patients [95]. The pericardial matrix induced neovascularization and the recruitment c-kit$^+$ cells [62].

A few other bio-derived materials have been examined for treating MI. Chitosan, a naturally occurring polysaccharide derived from crustacean shells, was injected with undifferentiated embryonic stem cells one week post-MI, resulting in improvement in EF, LV ED and ES diameters compared to the acellular scaffold, cell transplantation alone or saline in a rodent MI model 4 weeks post-injection [48,49]. The co-injection of a chitosan with bFGF improved EF, FS, LV diameters, and arteriole density as well as decreased infarct size and fibrotic area compared to the injection of bFGF alone 4 weeks post-transplantation in a rodent MI [50]. Similarly, gelatin with bFGF has shown improvements in cardiac function in both small [51] and large animals [52]. Injection

of Matrigel alone immediately post-infarction led to increased infarct wall thickness, improved EF as well as increased capillary density and c-Kit$^+$ cells when compared to saline in a rat MI model, 4 weeks post-injection [56]. Laflamme et al., injected human embryonic stem cell-derived cardiomyocytes in a multi-component pro-survival cocktail containing Matrigel in a rat occlusion-reperfusion model 4 days post-MI. After 4 weeks the pro-survival factors resulted in significantly increased cell survival. In addition, injection of this combination led to attenuation of LV remodeling post-MI as demonstrated by reduced ventricular dilation, improved global cardiac function and increased wall motion [57]. In addition, delivery of acellular calcium hydroxyapatite into an ovine MI model, led to improvement in EF and LV volume compared to the control 4 weeks and 8 weeks post-MI as well as a decrease in infarct expansion and longitudinal stain [69,70].

In the past five years, synthetic injectable polymers have begun to be examined as a treatment for MI. In contrast to biologically derived materials, synthetic materials allow for control over properties such as degradation, stiffness, porosity and gelation time, and do not suffer from the batch-to-batch variability that occurs with bio-derived materials. A matrix metalloproteinase-degradable poly(ethylene glycol) (PEG) loaded with thymosin ß-4 and endothelial (0.66×10^6 cells) and smooth muscle like (0.33×10^6 cells) cells derived from human embryonic stem cells improved EF, ED and ES volumes as well as decreased infarct size and increased vessel density compared to the control [73]. A similar

result was seen with injection of degradable poly(N-isopropylacrylamide) [78,80,81]

and PEG [75,76] based gels with or without cells in a MI. Garbern et al. injected a

pH-and temperature responsive hydrogel loaded with bFGF immediately post-MI

in a rat and showed a 30% to 40% increase in vessel density as well as an increase

in FS compared to the hydrogel alone and bFGF injected in saline 28 days post-

treatment [79]. Similarly, delivery of erythropoietin with a PEG-based gel into a rat

immediately post-MI led to an improvement in FS and LV ED and ES diameters

compared to injection of polymer alone and erythropoietin alone; however, all

groups demonstrated improvement compared to saline, 30 days post-MI [77]. Along

the same lines, VEGF was either mixed or conjugated to a hydrogel for delivery

into a rat one week post-MI. At 35 days post-injection, EF, ED and ES volumes,

scar thickness and vessel density were improved in the group where the VEGF

was tethered to the hydrogel when compared to the animals injected with

unconjugated VEGF, hydrogel alone and saline [74]. Thus, indicating that tethering

growth factors to biomaterials can lead to greater beneficial effects.

Poly(NIPAAM-co-acrylic acid) hydrogels with matrix metalloproteinase

degradable crosslinkers were used to transplant bone marrow derived

mononuclear cells (2×10^5 cells) into infarcted mouse myocardium. However,

injection of the material alone led to the greatest improvement in EF [82]. In the

past, Wall et al. used computational modeling to suggest that the presence of a

material alone at the site of infarction may lead to an improvement in cardiac

function due to an increase in wall thickness leading to a subsequent decrease in

wall stress due to Laplace's Law [96]. In order to study the effect of a non-degradable material on pathological remodeling, Dobner et al. injected a non-degradable PEG hydrogel immediately post-MI in a rat model. While LV ED diameter was reduced and wall thickness was increased at 4 weeks, by 13 weeks pathological progression was similar to that of saline injected animals [71]. Material properties of injectable biomaterials have recently come under investigation; Ifkovits et al. examined the effect of material stiffness on cardiac function and LV remodeling in an ovine MI model. Methacrylated hyaluronic acid was tailored to a stiffness of 8 kPa and 43 kPa and injected into the infarct 30 minutes post-MI. While there were no significant differences in functional parameters, infarct area was reduced in the group injected with a stiffer hydrogel at 8 weeks [64]. Another study injected a gel comprised of hyaluronic acid and PEG in a 2 week rodent MI and showed a clear improvement in EF and elastance compared to the control animals 4 weeks post-treatment [63]. However, the stiffness of the gel was not measured, so it is difficult to compare the results of this study with those of Ifkovits et al.

Bio-inspired self-assembling peptide nanofibers have been used as a platform for cell and growth factor delivery in both small [65,68] and large animals [66]. Davis et al. demonstrated that tethering insulin-like growth factor-1 to peptide nanofibers along with neonatal cardiomyocytes (5×10^5 cells) improved systolic function in a rat MI 21 days post-infarction compared to untethered growth factor [68]. Following this study, Lin et al. injected mini pigs with autologous bone

marrow mononuclear cells, peptide nanofibers (1% in saline) or a combination of both at the site of infarction immediately post-MI. Injection of cells with the nanofibers improved both diastolic and systolic function [66]. Most recently, self-assembling peptides were utilized for dual delivery of platelet derived growth factor and fibroblast growth factor 2 into a rat infarct, showing reduction in infarct size in addition to an increase in capillary and arteriole density at 4 and 8 weeks post-MI [67].

1.5 Conclusions

Over the last decade, many advancements have been made in the field of injectable biomaterials for the treatment of MI. Most notably, cardiac patch and injectable biomaterial treatments have reached the clinical trial stage and are showing promising outcomes in initial Phase I safety and feasibility trials [18,46]. Moreover, in recent years new materials have been developed for myocardial tissue engineering most significantly, synthetic materials and decellularized extracellular matrices. Remarkably, most biomaterials – cellular or acellular have led to an improvement in cardiac function and increased neovascularization. In the last couple years, we have begun to take steps towards understanding the biomaterial properties that influence cardiac function. A recent study assessed the effect of changing material mechanics; showing injection of stiffer materials to be beneficial for reducing infarct size [64]. However, many other design parameters for biomaterials are yet to be understood, such mechanical augmentation of the LV

wall by a passive structural support as well as the effect of material degradability on cardiac function and LV remodeling.

A majority of the biomaterials that have been examined are degradable, most with degradation rates ranging from one to eight weeks. After MI, collagen type I decreases from 80% to 40%, thus creating a need for structural reinforcement in the vulnerable tissue during early MI[97]. In addition, many of these materials are inherently bioactive and contain domains for cell adhesion or are modified with peptide sequences to promote cell adhesion and infiltration. While biomaterials may function as a structural support at early time points to prevent wall thinning, these polymers may also allow for cellular infiltration and adherence. These cells may be advantageous for changing the infarct milieu by increasing neovascularization, modulating the inflammatory response, and/or generating other positive paracrine factors.

Transplantation of cells can disrupt normal electrical propagation and increase arrhythmia vulnerability [98]. Similarly, concerns have been raised regarding the effect of injectable materials and cardiac patches on cardiac conduction. To date, there is a paucity of studies aimed at understanding the effect of biomaterial injection on action potential propagation and arrhythmogenesis, essential criteria for the safe translation of such therapies to humans.

Thus, there are still many gaps in current knowledge, with respect to the properties of biomaterials that are essential for improving cardiac function post-MI as well as criteria for delivery. With the advent of *in situ* gelling biomaterials,

allowing for minimally invasive modes of delivery, the accessibility to this emerging treatment should increase. As we move to human application it is exceedingly important that we understand the mechanism by which these materials influence LV remodeling, cardiac function, and how best to tailor future therapies to maximize their efficacy.

1.6 Scope of dissertation

The goal of the dissertation is to investigate the mechanisms by which injectable materials influence the damaged myocardium and understand the important and influencing properties that contribute to the beneficial effects seen with existing experimental injectable biomaterials for MI treatment. In specific, the effect of permanent passive structural enhancement and polymer degradation on cardiac function was studied, along with the effect of polymer injection on cardiac arrhythmogenesis. This work provides guidelines and considerations for the design and development of future biomaterial therapies for cardiac tissue engineering.

Chapter 1 provides an overview on the current state of injectable biomaterials and cardiac patch-based approaches for the treatment of MI.

Chapter 2 demonstrates that a permanent increase in wall thickness by injection of a bio-inert non-degradable material is insufficient to improve cardiac function and post-MI remodeling in a permanent occlusion MI model.

Chapter 3 describes the effect of intramyocardial injection of bio-inert degradable material on negative LV remodeling after an occlusion-reperfusion infarction. The findings from this study show that injection of a degradable biomaterial alone did not influence cardiac function and perhaps the ability for protein adsorption and cell adherence as seen with previously injected cardiac biomaterials may be an influential factor in prevention of post-MI LV remodeling.

Chapter 4 evaluates the effect of bulk and dispersed biomaterial injection in viable LV myocardium on cardiac action potential propagation and arrhythmogenesis, demonstrating that injection of a bulk biomaterials leads to delays in activation and a greater heterogeniety in action potential duration and repolarization – a possible cause for reentrant arrhythmia.

Chapter 5 provides a summary and conclusion of the work presented in this thesis and addresses future considerations for the development of new cardiac biomaterials as well as limitations of the presented work.

Chapter 1, in part is a reprint of material that is published as: Rane AR, Christman KL. Biomaterials for the treatment of myocardial infarction a 5-year update. J Am Coll Cardiol, 2011; 58 (25): 2615-29

Chapter 1, in part, is in submission as: Rane AR, Watson J, Christman KL. Tissue engineering and applications for treatment of myocardial infarction.

Chapter 1, in part, is a reprint of material that is published as: Rane AR, Chuang JS, Shah A, Hu DP, Dalton ND, Gu Y, Peterson KL, Christman KL.

Increased Infarct Wall Thickness by a Bio-inert Material is Insufficient to Prevent Negative Left Ventricular Remodeling after Myocardial Infarction. PLoS ONE, 2011; 6 (6): e21571.

The author of this dissertation is one of the primary authors or co-author on all publications.

CHAPTER TWO:

Increased infarct wall thickness by a bio-inert non-degradable material is insufficient to prevent LV remodeling after MI

2.1 Introduction

Progressive LV remodeling occurs after MI, and while remodeling can be beneficial initially, over time it can become maladaptive leading to LV dysfunction [2]. With 5.8 million people suffering from HF, treatment of negative LV remodeling after MI, the leading cause of HF, is a pressing clinical need [99].

Various injectable biomaterials have been investigated as potential acellular treatments to prevent or reverse this downward spiral of adverse LV remodeling [5]. Collagen [55], fibrin [100], chitosan [48], small intestinal submuscosa (SIS) [59], and a collagen-matrigel blend [58] as well as a few degradable synthetic materials [75,78,80] have shown either an improvement or maintenance of cardiac function in terms of EF or fractional shortening. Though most injectable materials have shown positive effects on cardiac function and LV remodeling, to date, the mechanisms behind this improvement are unknown.

It has been shown that myocardial infarction can lead to an increase in wall stress due to changes in wall curvature and thickness in accordance with Laplace's Law, which states that wall stress is directly proportional to the pressure and radius, and inversely proportional to thickness. Wall thinning due to infarction can increase wall stress, and may contribute to border zone expansion and progression of negative LV remodeling [101]. Hence, it has been hypothesized that injectable materials may affect the passive structural properties of the wall by increasing infarct wall thickness and hence reducing local LV wall stress [5,96]. This decrease in LV wall stress is thought to protect the vulnerable myocardium from

stress induced apoptosis and infarct expansion, thus preventing pathological LV remodeling and decline in cardiac function [96]. On the other hand, injectable materials have also been shown to elicit cell infiltration [53,102,103] and neovascularization [53] in the affected area. This leads to the alternate hypothesis that the bioactivity of materials, such as inherent cell adhesion domains or angiogenic degradation products, and/or cell infiltration upon degradation of these materials are playing an important role in prevention of adverse LV remodeling and improvement of cardiac function [5,104,105].

The aim of this study was to begin to understand the mechanisms by which injectable materials preserve cardiac function and prevent negative LV remodeling post-MI by decoupling bioactivity from the structural effects of an injectable polymer. Herein, we utilized an injectable, bio-inert, non-degradable polymer, polyethylene glycol (PEG), along with experimental parameters similar to those employed in previous studies aimed at assessing the effects of injectable biomaterials on LV remodeling and cardiac function. PEG is a well established synthetic polymer that is known to be non-toxic [106] and bio-inert, thus preventing protein and cell adhesion [106-109]. We demonstrate that passive structural intramyocardial support by itself does not prevent negative LV remodeling or maintain cardiac function, suggesting that other mechanisms such as bioactivity and/or cell infiltration seen with degradable materials likely play a dominant role in the mitigation of LV remodeling and preservation of cardiac function.

2.2 Methods

All experiments in this study were conducted in accordance with the guidelines established by the Institutional Animal Care and Use Committee at the University of California, San Diego and the American Association for Accreditation of Laboratory Animal Care and were approved by the Institutional Animal Care and Use Committee at UCSD (A3033-01). All efforts were made to minimize any pain and suffering felt by the animals.

2.2.1 PEG hydrogel preparation

PEG hydrogels were prepared by mixing solutions of 4-arm polyethylene glycol-amide-succinimidyl glutarate (Sunbio, Anyang City, South Korea, MW 20,000) and trilysine (Sigma-Aldrich, St. Louis, MO) to create non-degradable PEG- amide-succinimidyl glutarate (PEG-ND) hydrogels of desired stiffness at room temperature by chemical crosslinking [110]. Optimal concentrations of PEG-ND and trilysine were experimentally determined to generate gels of stiffness similar to that of commonly injected biomaterials. Equal volumes of 100 mg/ml PEG-ND in pH 4.0 phosphate buffer and 0.5 – 2 mg/ml trilysine in pH 8.2 borate buffer were mixed together to prepare the hydrogels. Trilysine (2mg/ml) was used with the same concentration of PEG to increase the stiffness of the hydrogel in the subsequent pilot study. For *in-vivo* injections of PEG, the solutions were mixed together and injected prior to gelation.

2.2.2 Mechanical testing

Material properties in terms of the storage modulus (G') and loss modulus (G") were determined using a parallel plate rheometer (TA Instruments AR-2000) as previously reported [111,112]. Briefly, gels were placed between two parallel plates of the rheometer and compressed to a normal force between 0.2 - 0.3 N, to avoid slipping. A strain sweep (0.0001 to 10%) was performed at a constant frequency of 1 Hz to confirm that the measurements were within the linear viscoelastic region. 1% constant strain was used for subsequent frequency sweeps (0.01 to 10 Hz) using a logarithmic scale, taking 5 points per decade. All measurements were taken in triplicate and reported as mean ± SEM at a frequency of 1 Hz.

2.2.3 Rat total occlusion model

Left coronary artery total occlusion was performed on female Sprague Dawley rats (225-250 g) under aseptic conditions. Animals were anesthetized using 5% isoflurane, intubated and maintained at 2.5% isoflurane for the surgical procedure. The animals were ventilated using a respirator at 75 breaths/minute. The heart was exposed using a left anterior thoracotomy, and the artery was ligated using a 6-0 silk suture at 1-2 mm below the left atrial appendage as previously reported [113]. The chest was closed and the animals were allowed to recover. ECG was continuously monitored for detection of arrhythmias, and

atropine 150 to 200 μl (0.54 mg/ml) was administered I.P. if needed. Buprenorphine was administered I.P. at 5 mg/kg to prevent post-operative pain and Ringer's Lactate (3 cc) was given I.P. to the animals to prevent dehydration.

2.2.4 Echocardiography

Echocardiography was performed 4 ± 1 day(s) post-MI to screen for the presence of an infarct. Animals were anesthetized using 5% isoflurane for 30 seconds and then maintained at 1% isoflurane for the imaging procedure. Parasternal long axis and short axis images were obtained using a Philips, Sonos 5500 system with a 15 MHz transducer. Qualitative assessment of infarction size was rendered at the time of imaging using both planes. Animals with either no MI or very small MI (less than 15% of the LV perimeter in the long axis plane) were excluded from the study prior to injections.

2.2.5 Injection surgery

The animals were randomized 9 ± 1 day(s) after MI, and injected with either 100 μl of PEG hydrogel or saline (control). An incision was made between the fourth and fifth ribs, the anterolateral portion of the heart was exposed, and an injection of polymer or saline was administered using a 27 G needle into the infarct wall. Presence of the injection was verified by temporary discoloration of the tissue. The chest was then closed and the animal was allowed to recover. To

prevent post-operative pain in the animals, buprenorphine was administered at 5 mg/kg.

2.2.6 Magnetic resonance imaging

Magnetic Resonance (MR) imaging was used for quantitative assessment of the injected gel on cardiac function. Animals were scanned at 7 ± 1 day(s) post-MI, as a baseline measurement, and again at 49 ± 4 days after MI to assess post-treatment effects on remodeling and cardiac function. A 7T Bruker Horizontal Bore scanner and Bruker single tuned quadrature Transmit/Receive volume coil were used for all measurements. Anatomical cine imaging was performed with an ECG-gated Fast Low Angle Shot (FLASH) sequence as previously reported [114]. MR parameters were set to TR = 7.7 ms, TE = 1.28 ms, flip angle = 15° and 4-6 averages per slice. All slices were 1 mm in thickness, had a field of view of 50 mm x 50 mm and were contained in a data matrix of 256 x 256 pixels. For each slice, 25 frames were taken through the cardiac cycle to capture end diastolic and end systolic images. Animals were anesthetized using 1.5 - 2% isoflurane and the heart rate, ECG and respiration rate were monitored continuously. The long axis of the heart was identified and 10-12 short axis slices from apex to base were acquired at 1 mm increments. ImageJ was used to trace the endocardial boundary at end diastole (ED) and end systole (ES) on each short axis slice. Simpson's method was used to determine the end diastolic volume (EDV) and end systolic volume (ESV). EF (EF) was calculated as [(EDV-ESV)/EDV] x 100 similar to

previous methods [115]. For Harmonic Phase (HARP) analysis, a Spatial Modulation of Magnetization (SPAMM) sequence was used for tagging of a short axis slice through the middle of the infarct, as previously shown.[116] A tagging thickness of 0.45 mm and tagging distance of 1.20 mm were used. All other parameters were the same as in the cine image acquisition.

2.2.7 Harmonic phase analysis

HARP analysis was used to track material points in SPAMM tagged images through the cardiac cycle.[117] Dependent on the cardiac gating, either the ED or ES frame of the SPAMM tagged image was converted into a frequency domain using a 2D Fast Fourier Transform (FFT). A bandpass filter with half the radius of the tagging frequency was used to isolate the spectral peak located at the first positive harmonic frequency in both horizontal and vertical tag directions. An inverse FFT of each spectral peak was taken to create a phase map of the material points. The phase pairs are time invariant and were used to track the material points through the cardiac cycle. The HARP analysis technique allowed for tracking displacement at the sub-pixel level.

2.2.8 Finite element modeling

In order to visually represent LV dilatation and wall thickness pre and post-injection, finite element analysis was used to generate geometric models of the LV at ED and ES using prolate spheroidal bi-cubic Hermite finite element

surface meshes [114]. Meshes were fit to the endocardial and epicardial boundary points determined from the MRI cine images. The boundary points were fit using a least squares minimization in the λ coordinate direction with bicubic Hermite interpolation. The 40 element mesh was refined to 340 elements and was converted to Cartesian coordinates so that the long axis of the heart aligned with the X- axis and the septum was bisected by the Y-axis.

For assessment of the area of akinetic tisuse, prolate spheroidal bi-cubic Hermite finite element surface meshes were made at ED and ES for each heart. The meshes were fit to the endocardial boundary points. The boundary points were also fit using a least squares minimization in the λ coordinate direction with bi-cubic Hermite interpolation. The meshes were refined from 16 to 340 elements. The distances between the nodes at ES and ED were calculated. Maps of the endocardial displacement from ED to ES were created by rendering the calculated distances on the end diastolic endocardial mesh. Akinetic tissue was determined as tissue having a value 10% or lower of healthy tissue displacement. Percentage of akinetic tissue was determined by calculating the surface area of the akinetic mesh elements with respect to the total surface area of the mesh.

For analysis of circumferential strain, a deformable finite element model was used to calculate circumferential strain in a short-axis slice through the middle of the infarct. ED was chosen as the undeformed reference state. Material points were obtained using HARP analysis on the SPAMM tagged images. The

materials points were fit from ED to ES using a least square fit of bi-cubic Hermite deformed nodal coordinate parameters for homogeneous strain analysis.

2.2.9 Histology and immunohistochemisty

Animals were sacrificed 24 hours after post-treatment MR imaging (~49 days post-MI) by an IP injection of Fatal Plus (sodium pentobarbital, 936 mg/kg). Hearts were immediately excised and fresh frozen in Tissue-Tek O.C.T. freezing compound. Hearts were sectioned into 10 μm slices and slides taken every 0.4 mm were stained with hematoxylin and eosin (H&E) to visualize the polymer injection. Images were taken using a Carl Zeiss Observer D.1 and analyzed using AxioVision software. A pathologist qualitatively assessed inflammatory response [118-120] to the injection in the infarct, border zone and remote tissue in the H&E stained sections at mid-infarct. Macrophages were identified using an anti-rat CD68 primary antibody.[121] Tissue sections were incubated with 1:50 dilution of mouse anti-rat CD68 and subsequently incubated with horseradish peroxidase (HRP) conjugated goat anti-mouse IgG (1:100 dilution). The HRP was visualized by incubation with diaminobenzidine (DAB) for 10 minutes. Wall thickness was calculated using 3 mid-infarct slides, averaging 5 equally spaced measurements along the infarct wall in each slide. Infarct size was calculated using H&E stained sections by calculating the average of the ratio of the endocardial infarct length to the endocardial circumference and the ratio of the epicardial infarct length to the epicardial circumference over three slides evenly spaced through the infarct as

previously shown [122]. To assess arteriole density, immunohistochemistry staining was done on three slides evenly spaced through the polymer region or infarct for each of the PEG and saline injected hearts respectively, according to previously described methods [39,92,103]. Briefly, the sections were fixed with acetone, incubated with anti-smooth muscle actin antibody and then stained with Alexa Fluor 568 anti-mouse antibody. Vessels in the range of 10µm to 100 µm in the infarct were quantified with Axiovision.

2.2.10 Statistical analysis

All data is presented as the mean ± standard error. For the Blyscan assay, samples were run in triplicate and results averaged, and reported using standard deviation. Significance was determined using a two-tailed student's t-test, and reported as $*p < 0.05$ and $**p < 0.01$. With the mitogenic assay, samples were run in quadruplicate and results were averaged.

2.3 Results

2.3.1 PEG hydrogel mechanical characterization

To create a PEG hydrogel with desired mechanical properties, the amount of trilysine crosslinker (0.5 mg/ml to 2 mg/ml) was varied. A strain sweep test and a frequency sweep test were performed to generate mechanical spectra of the gels. We sought to test a polymer with similar mechanical properties to commonly injected materials to better delineate between structural effects and

bioactivity. A storage modulus (G') of 0.5 ± 0.1 kPa (trilysine 1 mg/ml) (Figure 2.1) was selected as it mimicked the mechanical properties of commonly injected polymers [123,124]. As expected the G' is independent of frequency and G'' (loss modulus) is weakly dependent on frequency [112,125].
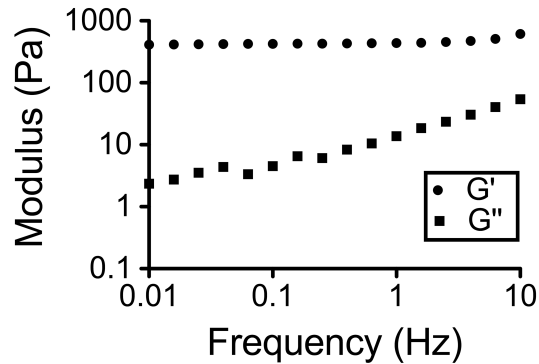
Figure 2.1: Mechanical spectra.
Typical mechanical spectra for a hydrogel formed by crosslinking of 4-arm PEG-ND (100 mg/ml) and trilysine (1mg/ml).

2.3.2 LV geometry and cardiac function

In-vivo studies were performed to assess the effect of the bio-inert, non-degradable PEG hydrogel on wall thickness, EF, EDV and ESV. All animals underwent a surgery to induce MI. After screening echocardiography, 17 out of 33 animals were included in the study based on presence of a sizable infarct. One additional animal died during intubation prior to injection. Sixteen animals therefore underwent either polymer (n=8) or saline (n=8) injections. 100% of the animals survived the injection surgery; however, 3 animals were removed from functional analysis, 2 animals from the saline group and 1 from the polymer group, due to inconsistent gating during MR imaging. These animals were

included in the histological analysis. One animal from the polymer group was excluded from the entire study due to insufficient polymer injection based on histology. In addition, infarct size was not different in the PEG (44.1 % ± 2.8 %) and saline (48.0 % ± 2.8 %) injected animals (p = 0.336).

Animals injected with the PEG hydrogel showed a significantly thicker infarct wall in comparison to saline injected animals (p= 0.006) as seen via histological analysis (Figure 2.2). Despite the increase in wall thickness, analysis of the MR images showed a steady decline in cardiac function and expansion of LV volume by comparing values pre- and post-treatment (Figure 2.3). At 7 weeks there was a significant increase in LV EDV (p=0.0016) and ESV (p= 0.0008), as well as a decrease in EF (p= 0.006) in the polymer group. As expected in the saline control group, LV EDV (p= 0.000002) and ESV (p=0.0001) significantly expanded with a corresponding decline in EF (p= 0.005). The heart rate of the animals was continuously monitored during the imaging process and was statistically similar between the PEG and saline injected groups: 278 ± 17 beats/min (PEG pre-injection) and 281 ± 8 beats/min (PEG post-injection); 271 ± 14 beats/min (saline pre-injection) and 285 ± 8 beats/min (saline post-injection). The ECG was carefully monitored during the time of image acquisition. There were no noticeable arrhythmias.

As a 3-D visual representation of the overall effect of polymer injection, finite element models were generated using the endocardial and epicardial boundaries traced from the MR images in ED (Figure 2.4). The overall change in

infarcted LV free wall thickness is seen pre- and post-injection (Figure 2.4,

arrows). The hearts injected with the PEG hydrogel demonstrated a regional

increase in wall thickness in the infarcted area while the saline injected hearts

showed a thinning of the infarct region at 7 weeks. Dilation of ventricle is clearly

depicted by enlargement of the LV lumen at 7 weeks as compared to baseline.
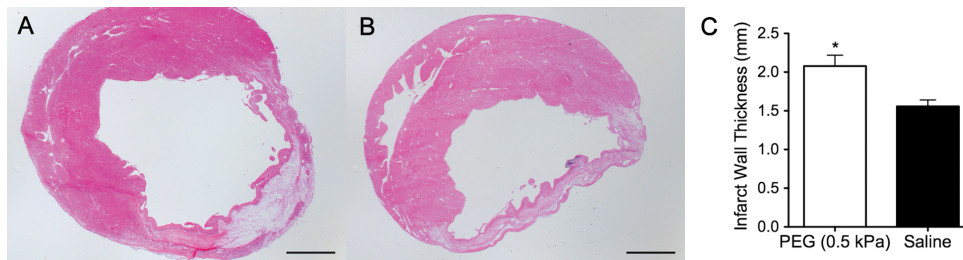
Figure 2.2: Histological assessment.
Histological assessment of polymer and saline injections 7 weeks after MI. Representative slides stained with H&E: (A) PEG hydrogel (G' = 0.5 kPa) injected in infarct region and (B) saline injected in infarct region. (C) Infarct wall thickness at 7 weeks post-MI. Wall thinning was prevented in the PEG injected group compared to the control. (*$p < 0.01$, PEG: n = 7, saline: n=8) Photomicrographs are taken at 10X and scale bars are 1mm. PEG area outlined with dotted line and demarcated by an asterisk (*).
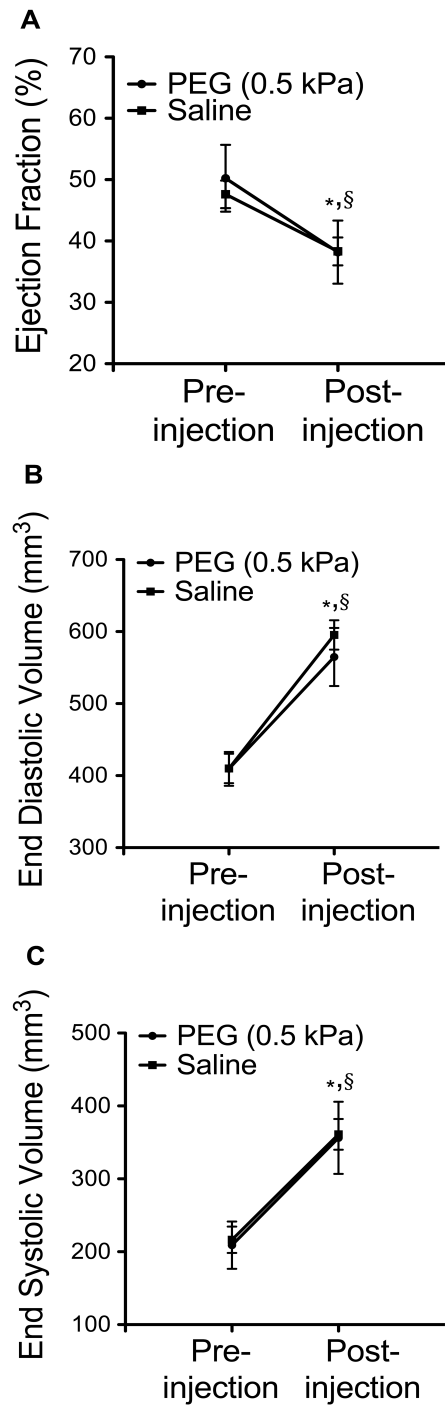
Figure 2.3: Cardiac function.
Comparison of cardiac function baseline (1 week post-MI, pre-injection) and post-treatment (7 weeks post-MI) in PEG (0.5 kPa) injected and saline injected groups. (A) Ejection fraction. (B) End diastolic volume. (C) End systolic volume. Statistical significance determined using paired two-tailed t-test between pre and post-injection groups. (*$p < 0.01$ PEG compared to baseline, § $p<0.01$ saline compared to baseline, PEG: n = 6, saline: n = 6)
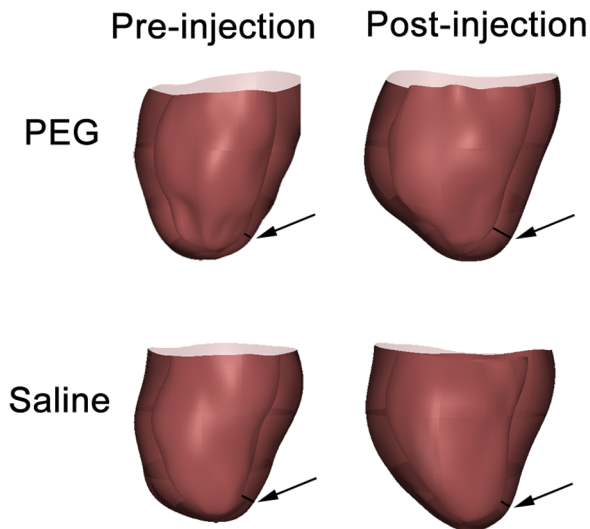
Figure 2.4: 3-D representation of the LV.
Finite element representation of the LV pre and post-injection in both PEG and saline injected groups. Arrow denotes region of infarction. Infarct wall thickening is seen in the PEG injected heart while infarct wall thinning is depicted in the saline injected heart compared to baseline. Also note the dilation of LV lumen pre and post-injection in both groups.

2.3.3 Regional cardiac function at mid-infarct

Rats injected with PEG gel showed a decrease in septal circumferential strain post-injection as compared to the pre-injection strain as can be seen qualitatively (values closer to zero – red/yellow) indicating impaired contractility in the septal region. On the other hand, septal dysfunction was not seen in the control rats (Figure 2.5).
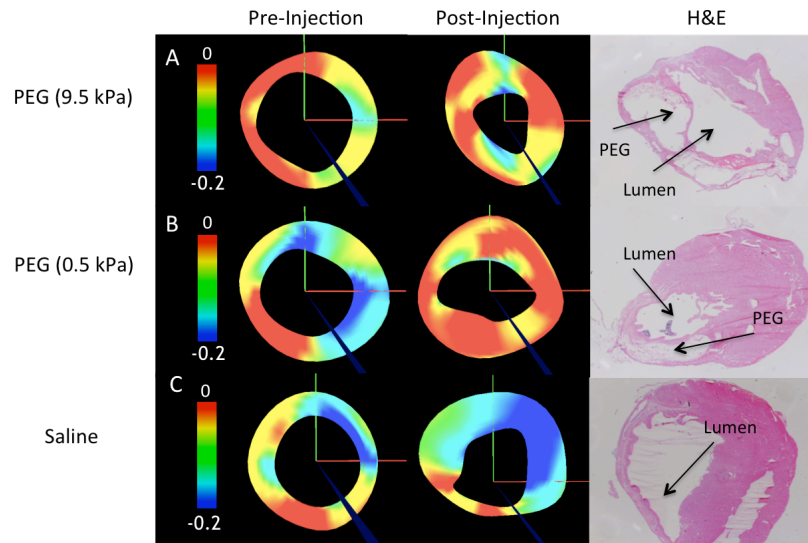
Figure 2.5: Regional circumferential strain.
Circumferential strain pre-injection, post-injection and H&E stained histology image (left to right) for stiffer PEG (A), more compliant PEG (B) and control (C) in a LV short axis section through mid-infarct. In these short axis slices the septal region is to the right of the section. There is a decrease septal circumferential strain in the PEG groups (A,B) post-injection indicating dysfunction.

2.3.4 LV akinesis

The region of impaired LV motion was identified by creating a finite element model measuring displacement of the endocardial boundary between end diastole and end systole. In Figure 2.6 the region in red denotes the endocardium with 10% or less displacement as compared to the normally contracting tissue. Analysis of LV akinesis indicates that in both the polymer and saline injected animals there is worsening of contractility in the ischemic portion of the LV at 7 weeks post-MI as well as infarct expansion in the control group. Similar results were seen in the polymer injected groups; however in these hearts the worsening

in contractility may be a combination of the non-contractility of the polymer as well as infarct expansion.
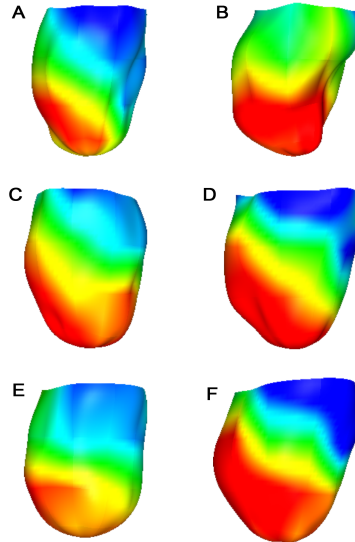
Figure 2.6: Endocardial displacement maps.
Representative endocardial displacement maps of stiff PEG, compliant PEG, saline pre-injection (A,C,E) and 6 weeks post-injection (B,D,F). Area in red denotes region of akinesis.

2.3.5 Cellular response to injection

As expected there was a very thin layer of encapsulation around the PEG injection region; however, there were no apparent differences in the inflammatory response (macrophages, fibroblasts, foreign body giant cells) between the polymer and saline injected animals in the infarct, border zone or remote myocardium as expected due to the bio-inert properties of PEG [106-109] (Figure 2.6 A,B). To further confirm this assessment, we examined the tissue for presence of CD68$^+$ macrophages and confirmed that there was no accumulation of macrophages in PEG injected hearts (Figure 2.6 C,D). Immunohistochemistry was performed on multiple sections through the hearts to assess the effect of polymer

injection on potential neovascularization in the infarct area. There was no significant difference in arteriole density for vessel diameters ranging between 10 µm and 100 µm in the infarct region of the polymer (19 ± 2 arterioles/mm^2) and saline (20 ± 2 arterioles/mm^2) injected hearts, or when vessels were binned as <10µm, between 10µm and 25µm, between 25µm and 50µm and between 50µm and 100µm, suggesting that polymer injection did not promote increased vessel formation (Figure 2.7).
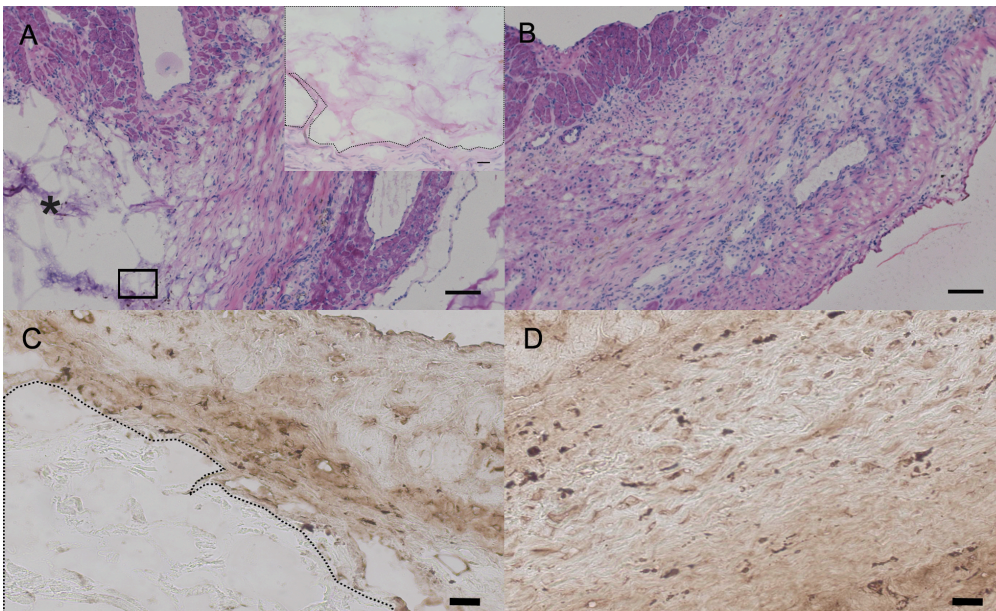
Figure 2.7: Inflammatory response.
Inflammatory response in polymer and saline injected hearts 7 weeks after MI. (A) PEG injected heart (inset shows high magnification image of PEG region showing no cell infiltration in the polymer, scale bar 20 µm) (B) saline injected heart. Scale bars are 100 µm. PEG area is demarcated by an asterisk (*). CD68 stained macrophages in (C) PEG injected heart (D) saline injected heart. PEG area outlined with a dotted line. Scale bars are 20 µm.
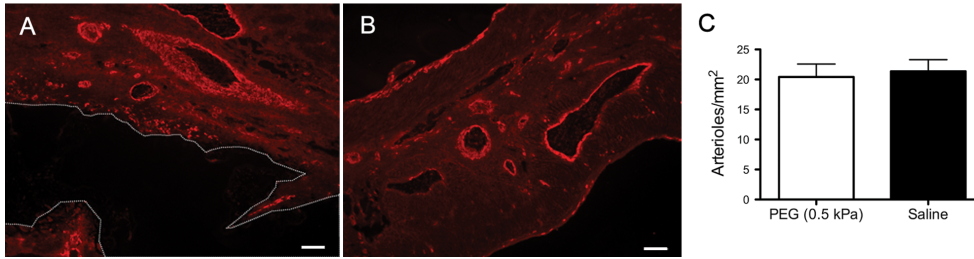
Figure 2.8: Arteriole density.
Arteriole density assessment in polymer and saline injected hearts 7 weeks after MI. (A, B) Representative slides with staining for smooth muscle actin. (A) Arterioles in infarct region of PEG injected animals. PEG area outlined with dotted line and demarcated by an asterisk (*). (B) Arterioles in infarct region of saline injected animals. Scale bars are 100 μm. (C) Arteriole density (vessel diameter between 10 μm and 100 μm) at 7 weeks post-MI. (p = 0.80, PEG: n = 6, saline: n=8)

2.3.6 Intramyocardial injection of 10 kPa polymer

Since a change in the mechanical properties of a material may affect its structural properties in the heart, a small pilot study was performed to assess whether a stiffer material with a modulus closer to that of the myocardium would prevent negative LV remodeling and preserve/improve cardiac function. A PEG hydrogel composition with a storage modulus of 9.5 ± 0.5 kPa, closer to that of the myocardium,[126] was therefore injected into rat infarcts using identical study parameters. After screening with echocardiography, 8 out of 17 animals were included in the study. Two animals died after injection and one animal died during post-injection imaging. Two animals were excluded because of insufficient polymer within the heart, and one animal was excluded from MRI analysis due to inconsistent ECG gating, but was included in histological analysis. As with the more compliant gel, this PEG also increased infarct thickness to 2.4 ± 0.3 mm at 7 weeks post-MI. Final MRI analysis was only performed on 2 rats; however, both had a decline in EF (62 to 54% and 45 to 25% for each rat

respectively) and increase in LV EDV (379 to 383 mm^3 and 423 to 739 mm^3) and ESV (142 to 177 mm^3 and 231 to 554 mm^3).

2.4 Discussion

To date, the exact mechanism by which injectable materials lead to an improvement in cardiac function is unknown. As most injectable biomaterials cause an increase in infarct wall thickness, some have hypothesized that this passive structural enhancement alone may have therapeutic benefit [5,96]. After MI, there is typically a thinning of the myocardial wall and replacement with scar tissue. According to the Law of Laplace, this thinning can cause an increase in wall stress that can cause infarct expansion and apoptosis of the myocytes, which in turn can lead to dilation of LV and subsequent HF [3,96]. Thus, it has been proposed that use of an injectable material to increase wall thickness may lead to a decrease in wall stress and hence prevent adverse LV remodeling [96]. Alternatively, bioactivity or degradation properties of biomaterials may lead to the beneficial effects of these materials in the post-MI setting. The majority of biomaterials that have been examined to date are degradable materials that allow for cell infiltration, as well as biopolymers that have inherent bioactivity. In an effort to begin to understand the mechanisms behind which injectable polymers improve cardiac function, we chose to examine a bio-inert, non-degradable synthetic polymer, PEG, to decouple a material's structural effects from its bioactivity. We chose a compliant gel that mimicked the mechanical properties of commonly injected polymers. Results from this study indicate that injection of

PEG leads to an increase in infarct wall thickness, consistent with what has previously been seen with other materials [44,55,78,100]. However, this was insufficient to prevent negative LV remodeling or improve cardiac function as determined through MRI. A strictly structural enhancement of the LV wall may therefore be insufficient for preservation or improvement of cardiac function and/or slowing the progression of negative LV remodeling after MI. In addition, regional strain analysis demonstrated a deterioration of function in the septal region upon addition of the polymer. These results therefore indicate that other properties of injectable biomaterials may be playing an important role in maintenance or enhancement of function post-MI.

In this study, we show that injection of the non-degradable PEG does not induce post-MI neovascularization, nor does it increase cell infiltration in general. In contrast, many previously injected materials that have shown improvement in cardiac function display increased neovascularization, possibly restoring the blood supply to the affected area and preventing negative LV remodeling [48,53,102]. The increase in new vessel formation could be due to bioactive components of the materials such as angiogenesis inducing degradation products (e.g. Fibrin fragment E [127] and peptide fragment hepIII of collagen IV [128]) Unlike PEG, most of these biomaterials also have integrin binding sites that are important for the influx of cells, such as endothelial cells and myofibroblasts [129]. Huang *et al* have shown that injection of collagen in the infarct induced significant myofibroblast infiltration. Similarly there was also a trend for increased myofibroblast

migration in fibrin and matrigel injected hearts [53]. It has been shown that the contractile nature of myofibroblasts may lead to infarct size reduction and mitigation of infarct expansion, leading to overall improvement in function [130]. In addition to biopolymers, beneficial effects with a few degradable synthetic polymers that allow for cell influx have also been observed [80]. Therefore, cell infiltration due to degradation of injected polymers might be a potential mechanism by which these materials elicit salutatory effects. Though this effect with biopolymers is likely a result of their inherent bioactivity, these materials have also been shown to degrade in the range of 1-6 weeks [48,53,92]. While most of these infiltrating cells cannot restore function to the damaged area, it is possible that the migration of these cells in a timely manner provides beneficial paracrine effects necessary to prevent or lessen infarct scar expansion that is commonly seen post-MI.

While most materials have been degradable, there is one report of a synthetic non-degradable polymer being used for treatment of MI; Dobner *et al* [71], injected a non-degradable PEG in the infarct immediately post-MI and showed that there was temporary retardation of LV remodeling at early time points, but not at later time points. However, the progression of LV remodeling at later time points is aligned with the presented results. It is challenging to make a direct comparison between this study and the presented work as the material properties of the PEG gel were not characterized, and the PEG was injected at a different time point. An additional study has also examined the effects of mechanical

properties of materials in an MI setting. Ifkovits *et al* [64], investigated the effect of mechanical modulation of injectable HA hydrogels on LV remodeling and cardiac function in an ovine MI model, finding a smaller infarct area in animals injected with the higher mechanical modulus HA. In that study, the HA spread more interstitially through the infarct, which could have contributed to the differences seen in the results of the presented work and the study performed by Ifkovits *et al*. However, similar to the results presented here, there was a reduction in EF in all groups compared to baseline. Furthermore, in a study by Garbern *et al*, a pH sensitive, temperature responsive synthetic polymer was injected with or without the addition of bFGF in a rodent infarct model. The control group injected with polymer alone increased infarct wall thickness, yet showed a steady decline in fractional shortening comparable to that of the saline injected control, indicating the polymer injection did not improve cardiac function [79]. While the polymer was designed to degrade, it did not degrade over the course of the study, thus providing additional evidence that degradation may be a key biomaterial parameter for preserving or improving cardiac function post-MI.

In the present study, MRI was the imaging modality of choice. It is well established that MRI is the gold standard for cardiac imaging [131,132]. Commonly, echocardiography is used for the measurement of cardiac function after injection of a biomaterial. Measurements are made at the level of the papillary muscles that function as an anatomical marker. In the commonly used total occlusion MI model, the anteroapical portion of the heart is most severely affected. The effects

of LV dilatation and systolic bulging are thought to be most pronounced in this region. It is possible that by taking measurements at one level the effect of LV dilatation distal to the papillary muscles is overlooked and local effects are being underemphasized. However, using MRI we were able to determine the overall effect of the polymer injection.

As elucidated here, there may be various factors that are potentially contributing to the beneficial effect seen with injectable materials post-MI. In order to better understand the role of biomaterials in MI treatment and compare our findings to previous work, the PEG polymer used in this study was specifically engineered to have properties similar to other previously examined injectable biomaterials. Moreover, we mimicked common study parameters such as the timing of injection and the injection volume. There are however some differences and limitations to our findings. For example, this PEG gels rapidly upon injection limiting the interstitial spread of the material, allowing it to serve as a bulk filler and partial wall replacement. One potential limitation may be the inability of the polymer bolus to distribute through the entire area of the infarct as seen with external LV restraints [133]. This inhomogeneity in spread could lead to regional abnormalities in function as well as allow for infarct expansion in regions where the polymer is not present. Moreover, there could also still be compensatory expansion of the non-infarcted LV that negates any structural support provided by the material injection. In larger animals, multiple injections can ensure more homogeneous spread of material, although 100% coverage of the

wall would still not be achievable. Despite the single injection in the majority of rodent experiments, injection of biomaterials have still improved or preserved cardiac function. In addition to injection spread, timing of injection may also be an important parameter. While some may argue at one week post MI the initial expansion of the ventricle has already occurred, most previous studies injected material in the infarct approximately 1 week post-infarction [41,44,48,53,55,92,100]. Injection at this time point also represents greater clinical translatability due to fear of ventricular rupture at earlier time points. In the literature, volumes of $50\mu L$ to $150\mu L$ have been injected in rat hearts [41,44,48,50,53,55,71,92,100,134,135], hence $100\mu L$ injection volume was selected as it falls in this range and is the volume used most frequently in biomaterial injection studies.

In conclusion, passive structural enhancement by injection of a synthetic, non-degradable polymer into a developing infarct did not improve global cardiac function and was insufficient to alter post-MI remodeling, thereby suggesting that the bioactivity and/or cell infiltration seen with degradable materials may likely play an important role in preserving cardiac function. The results of this study provide additional insight on the important and influencing properties of biomaterials necessary for preventing post-MI negative remodeling. Furthermore, this study highlights the need for further studies that closely examine biomaterial parameters in order to guide the design of enhanced biomaterials therapies for MI.

Chapter 2, in part, is a reprint of material that is published as: Rane AR, Chuang JS, Shah A, Hu DP, Dalton ND, Gu Y, Peterson KL, Omens JH, Christman KL. Increased Infarct Wall Thickness by a Bio-inert Material is Insufficient to Prevent Negative Left Ventricular Remodeling after Myocardial Infarction. PLoS ONE, 2011; 6 (6): e21571.

The author of this dissertation is one of the primary authors on this publication.

CHAPTER THREE:

Intramyocardial injection of bio-inert degradable PEG does not prevent adverse LV remodeling post-MI

3.1 Introduction

It was widely thought that mechanical augmentation of vulnerable myocardium could reduce wall stress and prevent infarct expansion and pathological remodeling. Nonetheless, based on the results in Chapter 2, passive structural support by injection of a non-degradable material was incapable of improving post-MI remodeling. Still, several biologically derived materials and a couple synthetic materials have shown beneficial effects with respect to cardiac function, LV geometry and cellular response [9]. Many of these biologically derived materials such as fibrin, collagen, Matrigel and decellularized tissues are composed of ECM components that contain bioactive peptides, which promote cellular recruitment. However, notable among both biological and synthetic biomaterials that have shown benefit, is their ability to degrade *in vivo*. Most of these materials degrade within a time scale 1 to 8 weeks [9]. The appropriate degradation of these materials may allow for cells to infiltrate into the infarcted myocardium in a timely manner and promote beneficial remodeling of the tissue.

Herein, we further investigate the mechanisms by which injectable materials preserve cardiac function and prevent negative LV remodeling post-MI by evaluating the effect of an injectable, non-bioactive, degradable material on cardiac function after infarction. As in Chapter 2, PEG was utilized because of the ease of tunability. The materials were tailored to exhibit similar physical properties but degradation rate was varied to generate hydrogels with different

degradation times *in vivo*. In addition, PEG resists protein and cell adhesion [106-109], providing the capability to decouple the physical characteristics of degradability of the PEG and any potential biological effects due to protein adhesion to the surface. We demonstrate that injection of a degradable PEG material leads to a worsening in cardiac function and LV geometry as well as contributes to adverse LV remodeling in a rat MI model. This suggests that other mechanisms are likely playing an important role in curbing negative LV remodeling and preserving cardiac function, such as cell adhesion and infiltration due to protein adsorption on the material surface or inherent bioactivity of the material.

3.2 Methods

3.2.1 PEG hydrogel preparation

PEG hydrogels were prepared by mixing solutions of 4-arm polyethylene glycol-amide-succinimidyl glutarate, 4-arm polyethylene glycol-succinimidyl glutarate or 4-arm polyethylene glycol-succinimidyl succinate and 4-arm polyethylene glycol-amine (PEG-NH$_2$) (JenKem, MW 20,000) to create PEG hydrogels of a required stiffness by chemical crosslinking [110]. Equal volumes of PEG glutarate or succinate in pH 4.0 phosphate buffer and PEG- NH$_2$ in pH 7.6 borate buffer were mixed together to prepare the hydrogels at 10 % (w/v). For injection *in vivo*, the PEG solutions were mixed together and injected prior to gelation (~20 seconds post-mixing).

3.2.2 Mechanical testing

The storage modulus (G') and loss modulus (G") were determined using a parallel plate rheometer as previously reported [72,111,112]. All measurements were taken in triplicate and reported as mean ± SEM at a frequency of 1 Hz.

3.2.3 Hydrogel swelling

Hydrogel swelling percentage was assessed for the PEG-ND, PEG-D and PEG-FD based hydrogels by placing 30 µL gels (n = 5 per group) in a 24-well plate and immersing in PBS. The plate was agitated for the duration of the experiments. The gels were removed at pre-determined intervals and their weight was calculated. Measurements were taken until equilibrium was reached. The percentage swelling was calculated as follows:

$$\% Swelling = \frac{(W_s - W_i)}{W_i} \times 100$$

Where W_s is the weight of the gel in the swelled state and W_i is the initial weight of the hydrogel prior to immersion in PBS.

3.2.4 Rat occlusion-reperfusion MI model

Left coronary artery temporary occlusion was performed on female Sprague Dawley rats (225-250 g) under aseptic conditions. Animals were anesthetized using 5% isoflurane, intubated and lowered 2.5% during incision

through the 2nd and 3rd ribs and subsequently lowered to 1.5% isoflurane for the rest of the surgical procedure. The animals were ventilated using a respirator at ~75 breaths/minute. The heart was exposed using a left anterior thoracotomy, and the artery was occluded for 25 minutes using a 6-0 silk suture at 1-2 mm below the left atrial appendage. The chest was closed and the animals were allowed to recover. The electrocardiogram was continuously monitored during the procedure for detection of arrhythmias. Buprenorphine was administered subcutaneously at 5 mg/kg to prevent post-operative pain and Ringer's Lactate (3 cc) was given subcutaneously to the animals to prevent dehydration.

3.2.5 *In vivo* degradation time assessment

To assess polymer degradation time, 75 µl of non-degradable PEG-amide-succinimidyl glutarate (PEG-ND), degradable PEG-succinimidyl glutarate (PEG-D) or fast degrading PEG-succinimidyl succinate (PEG-FS) based gels were injected *in vivo* in a rat MI model one week after infarction and the animals were sacrificed at 2 weeks, 3 weeks and 4.5 weeks post-injection. Histological sections were taken and stained using Masson's trichrome. Presence of the PEG was visually detected in the histological sections.

3.2.6 Echocardiography

Transthoracic echocardiography was performed one week post-MI to screen for the presence of an infarct and perform baseline measurements of

cardiac function. Animals were anesthetized using 5% isoflurane and then maintained at 1% isoflurane during the imaging procedure. Parasternal long axis and short axis images were obtained using a GE Vivid i system with a 12 MHz transducer. Qualitative assessment of infarction size was rendered at the time of imaging using both planes. Animals with either no MI or very small MI were excluded from the study prior to injections. If the animal was included in the study, a full set of measurements including LV internal diameter, areas and volumes were taken. Ejection fraction (EF), fractional area change (FAC) and fractional shortening (FS) were calculated using LV volumes, areas and lengths respectively. Volumes and subsequently, EF was measured using the method of disc. Echocardiographic measurements were performed again 5 weeks post-MI and the same parameters were assessed for post-treatment comparison of cardiac function between groups and pre-injection/post-treatment comparison with in each group. The heart rate of the animals was continuously observed and the ECG was carefully monitored during image acquisition to ensure there were no noticeable arrhythmias. An experienced sonographer who was blinded to the treatment groups performed all image acquisition and analysis.

3.2.7 Injection surgery

The animals were randomized one week after MI, and injected with either 70 – 75 μl of PEG-ND (n = 12), PEG-D (n = 13), or saline (n = 12) (control). The rats were anesthetize with 5% isoflurane, intubated and maintained at 1.5 to 2.5%

for the entire surgical procedure. A lateral incision was made in the abdominal region below the xyphoid process, followed by an incision through the diaphragm. The pericardium was partially removed and the anterolateral portion of the heart was exposed. An injection of material or saline was administered using a 27 G needle into the infarct wall. Presence of the injection was verified by temporary discoloration of the tissue. The chest was then closed and the animal was allowed to recover. To prevent post-operative pain in the animals, buprenorphine was administered at 5 mg/kg subcutaneously and Lactate Ringer's were given to prevent dehydration as was done in the MI surgery.

3.2.8 Histology and immunohistochemistry

Animals were sacrificed immediately after post-treatment echocardiography (5 weeks post-MI) by an IP injection of Fatal Plus (sodium pentobarbital, 936 mg/kg). Hearts were immediately excised and arrested in a solution containing 25 mM $NaHCO_3$, 2 mM $CaCl_2$, 5 mM Dextrose, 2.7 mM $MgSO_4$, 22.8 mM KCl, 121.7 mM NaCl, 20 mM 2,3 butanedione monoxime. They were subsequently fresh frozen in Tissue-Tek O.C.T. freezing compound and sectioned along the short axis, using a cryostat into 10 μm slices with slides taken every 0.42 mm. The slides were stained with Masson's trichrome to visualize the infarct region (blue) and polymer injection (brown). Images were acquired and analyzed using AxioVision software. Wall thickness was calculated as previously shown [72]. Scar thickness calculated using 3 mid-infarct slides,

averaging 5 equally spaced measurements of the scar length in the radial direction for each slide.

Scar area percentage was calculated as the ratio of the infarct area to total LV area (septum included) multiplied by 100. All areas were obtained by outlining the respective regions on three trichrome stained images (10X) spaced evenly through the infarcted region of the heart. Infarct size was assessed over the same slides as the scar area, as previously shown [122]. The average of the ratio of the endocardial infarct length to the endocardial circumference and the ratio of the epicardial infarct length to the epicardial circumference multiplied by 100 was taken as the infarct size.

To assess arteriole density, immunohistochemistry staining was done on three slides evenly spaced through the infarct region, according to previously described methods [39,92,103]. Briefly, the sections were fixed with acetone, blocked and incubated with anti-smooth muscle actin antibody and then stained with Alexa Fluor 568 anti-mouse antibody. Vessels in the range of 10μm to 100 μm in the infarct were quantified using Axiovision. Sections were also stained for macrophage infiltration. Myofibroblasts were quantified as on the same slides as non-vessel alpha-smooth muscle actin stained cells. M0 macrophages were identified with a mouse anti-rat CD68 antibody (AbD Serotec, Raleigh, NC) and M2 macrophages were identified with a mouse anti-rat CD163 antibody (Santa Cruz Technologies, Santa Cruz, CA). Both primary antibodies were used at a dilution of 1:100. A horseradish peroxidase conjugated anti-mouse IgG

secondary antibody was used at a dilution of 1:500 (Millipore, Billerica, MA). The reaction was visualized with a metal enhanced diaminobenzidine (DAB) substrate kit (Thermo Fisher Scientific, Rockford, IL) according to manufacturer's instructions. Stained sections were imaged using a 20x objective (200x magnification). The infarct was identified and 3-5 evenly spaced images were taken on three slides evenly spaced through the infarct. Macrophages in each field of view were counted and averaged per area for each heart. A ratio of M2 to M0 macrophages was calculated.

3.2.9 Statistical analysis

Differences between baseline and post-treatment echocardiographic measures were assessed using a paired two-tailed t-test in addition to a two-way Analysis of Variance (ANOVA) followed by bonferroni post-hoc analysis. All other statistical analysis was performed using one-way ANOVA followed by a Newman-Keuls post-hoc analysis. All measurements were reported mean ± SEM, other than where specifically stated. Significance was accepted at $p < 0.05$.

3.3 Results

3.3.1 PEG hydrogel characterization

PEG hydrogels were created by crosslinking PEG-ND with PEG-NH$_2$ to create a non-degradable hydrogel. Alternatively PEG-D or PEG-FD were crosslinked with PEG-NH$_2$ to create a degradable hydrogel. The stiffness, in

terms of storage modulus, of the gels was measured using parallel plate rheometry and all the PEG hydrogels had a storage modulus on the order of 10 kPa (PEG-ND: 8.9 ± 1.5 kPa, PEG-D: 13.4 ± 2.7 kPa and PEG-FD: 8.8 ± 1.7 kPa) (Figure 3.1). A stiffness of ~10 kPa was selected as it is in the range of commonly injected biomaterials such as alginate [136] and fibrin [137] and on the same order of magnitude as healthy myocardium [64,126]. As previously demonstrated, the G' (storage modulus) was independent of frequency and G'' (loss modulus) was weakly dependent on frequency [72]. The swelling characteristics were also similar between the PEG-ND and PEG-D with the PEG-ND gel swelling to a maximum of 221.0 % ± 17.0 % and PEG-D to a maximum of 183.7 % ± 22.5 % (Figure 3.2). The PEG-FD hydrolyzed before reaching a plateau in the swelling curve; the maximum measurable swelling was ~ 450%. Degradation time of the PEG-based polymers was qualitatively assessed *in vivo* in a rat occlusion-reperfusion MI model. PEG-FD was largely degraded 3 weeks post-injection and only minimal remaining PEG-D was visualized at 4.5 weeks. The PEG-ND remained without degradation in the tissue up to the end point of the study (4.5 weeks), similar to our previous study [72]. For the *in vivo* assessment of cardiac function PEG-D and PEG-ND were selected as the degradable and non-degradable polymers respectively since they most closely resembled each other in terms of chemical and physical properties.

A

B

C
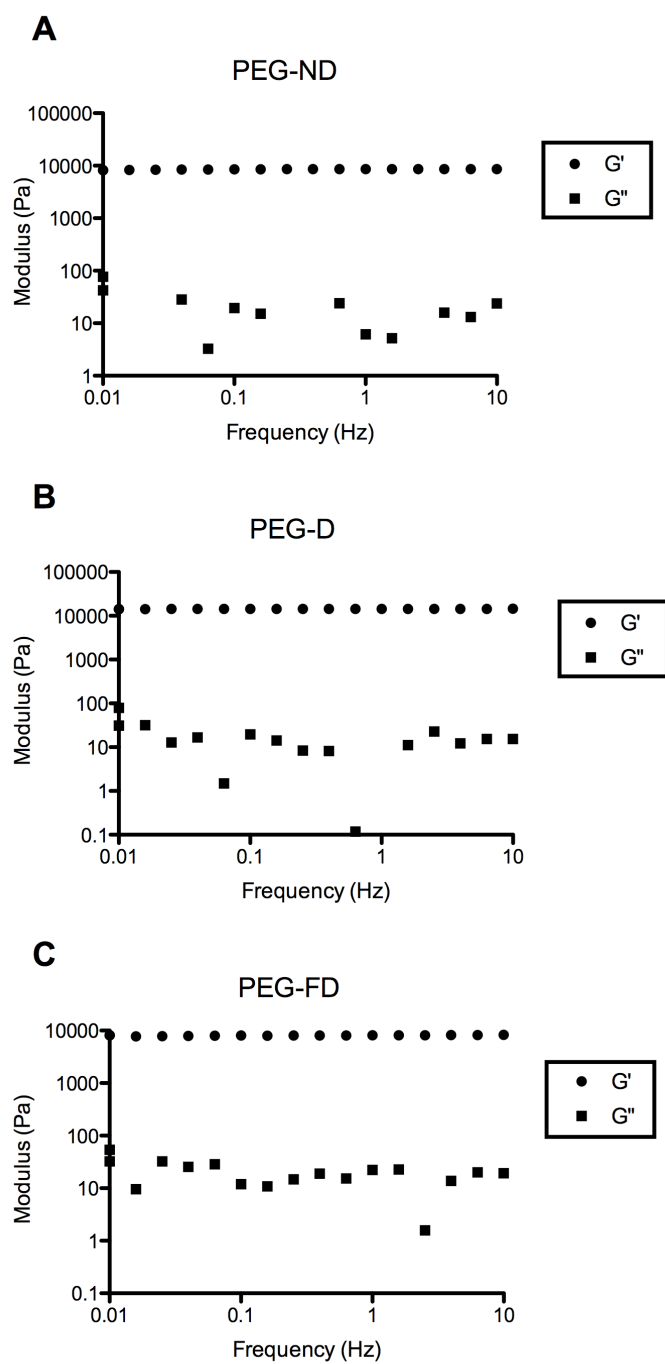
Figure 3.1: Mechanical spectra for PEG hydrogels.
Typical mechanical spectra for a hydrogels formed by crosslinking of 4-arm PEG-ND (A), PEG-D (B) and PEG-FD (C) with 4-arm PEG-NH$_2$.
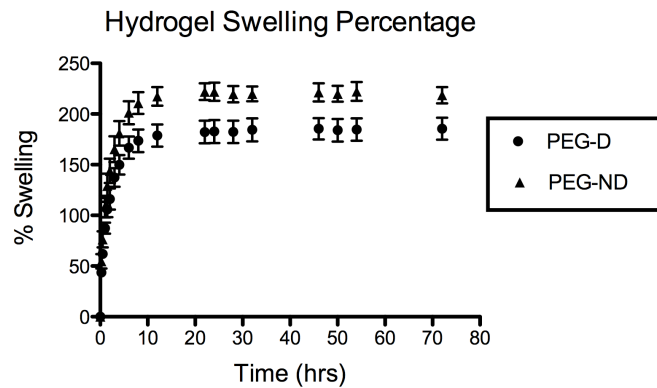
Figure 3.2: Hydrogel swelling percentage.
Hydrogel swelling curve for (A) PEG-ND and (B) PEG-D hydrogels.

3.3.2 Cardiac function

In vivo studies were performed in a rat occlusion-reperfusion MI model to assess the effect of a bio-inert, degradable PEG hydrogel compared to a non-degradable PEG, and a saline control on global cardiac function. One week later echocardiographic measurements were taken as a baseline for comparison to post-treatment measurements. Animals with a very small or no infarct were excluded from the study. After the baseline and screening echocardiography 45 animals underwent an intramyocardial injection of PEG-D (n = 13), PEG-ND (n = 12), or saline (n = 12) injections. Two animals from the PEG-D group and three animals from the saline group were excluded due to lack of infarction upon histological analysis.

Histological measurements were performed on the excised hearts after the post-treatment echocardiography. The scar area was significantly increased in the PEG-ND (23.3 ± 3.1 %) injected hearts compared to the PEG-D (13.9 ± 2.7 %)

and saline (7.8 ± 2.5 %) injected hearts (Figure 3.3 E). The scar area in the PEG-D injected hearts showed a trend towards being greater than scar area in the hearts injected with saline. The infarct size in the PEG-ND group was larger than the saline injected group, though all groups showed similar trends to the scar area data (PEG-ND: 43.1 ± 4.5 %, PEG-D: 34.8 ± 4.1 %, saline: 24.1 ± 4.1 %) (Figure 3.3 F). The wall thickness was statistically similar in the PEG-ND, PEG-D and saline injected animals, however the scar thickness in the PEG-ND group was greater than all other groups (Figure 3.4).

Functional outcomes were measured using echocardiography and post-treatment measures were compared to baseline (Table 3.1). The PEG injected animals showed a decline in EF and FS 5 weeks post-MI (4 weeks post-treatment). Similarly, there was an increase in LV volumes in the saline and PEG injected hearts. Post-treatment comparison of echocardiographic measures demonstrated that LV geometry was negatively impacted by the injection of both the degradable PEG and non-degradable PEG when compared to saline (Table 3.1).
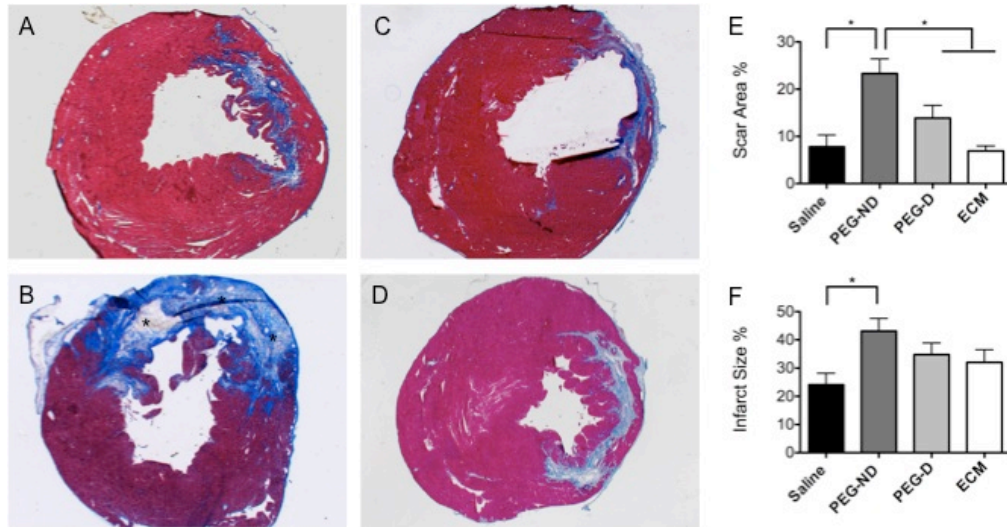
Figure 3.3: Scar area and infarct size

Representative histological section of (A) saline, (B) PEG-ASG * denotes region of polymer spread, (C) PEG-D and (D) ECM injected hearts. Scar area percentage is shown in (E). The PEG-ND group has a significantly increased infarct size compared to saline, PEG-D and ECM injected animals. Infarct size is also increased in the PEG-ND group compared to saline. * P <0.05. (ECM data was provided courtesy of Sonya Seif-Naraghi, Department of Bioengineering, University of California San Diego)
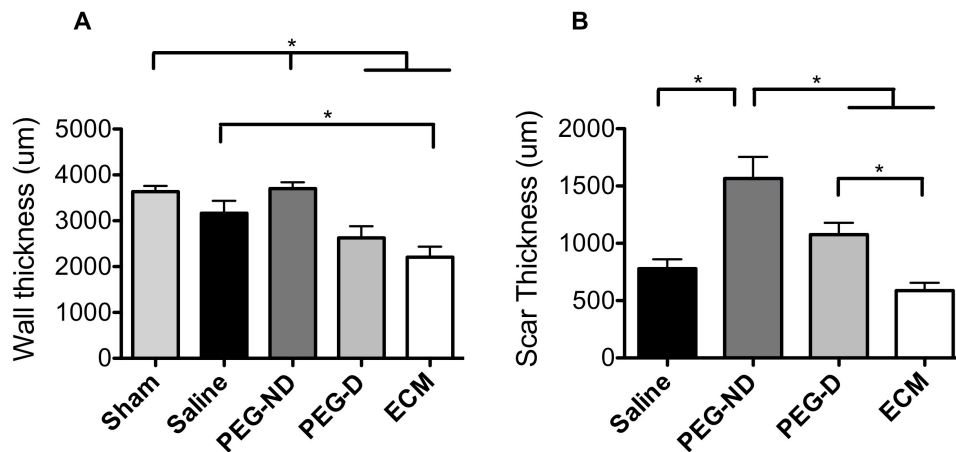
Figure 3.4: LV wall thickness and scar thickness.

Graphical representation of the (A) wall thickness and (B) scar thickness in 5 weeks post-MI. The wall thickness in the sham and PEG-ND injected animals is significantly greater than the PEG SG and the ECM injected animals, while the wall thickness in the saline animals is greater than the ECM animals. The scar thickness in the PEG-ND group is larger compared to all other groups. In addition, the scar thickness in the PEG-D animals is greater than that in the ECM animals. *P < 0.05. (ECM data was provided courtesy of Sonya Seif-Naraghi, Department of Bioengineering, University of California San Diego)

Table 3.1: Echocardiography functional study

	Saline n = 9	PEG-ND n = 12	PEG-D n = 11	ECM n = 8	Sham n = 8
LVIDd (cm)					
Baseline	0.61 ± 0.08	0.62 ± 0.07	0.65 ± 0.06	0.65 ± 0.04	0.61 ± 0.04
4 weeks	0.66 ± 0.08	0.74 ± 0.09 [*, ††]	0.71 ± 0.09	0.65 ± 0.05	
p	0.105	0.008	0.088	0.936	
LVIDs (cm)					
Baseline	0.40 ± 0.05	0.41 ± 0.07	0.42 ± 0.04	0.43 ± 0.05	0.41 ± 0.04
4 weeks	0.45 ± 0.08	0.55 ± 0.12	0.51 ± 0.11	0.45 ± 0.05	
p	0.019	0.0002	0.019	0.240	
LVAd (cm^2)					
Baseline	0.28 ± 0.06	0.30 ± 0.04	0.34 ± 0.08	0.31 ± 0.04	0.31 ± 0.04
4 weeks	0.35 ± 0.06	0.43 ± 0.14	0.49 ± 0.14 [*, †, ††]	0.34 ± 0.06	
p	0.001	0.011	0.003	0.280	
LVAs (cm^2)					
Baseline	0.12 ± 0.04	0.10 ± 0.04	0.16 ± 0.09	0.12 ± 0.03	0.10 ± 0.03
4 weeks	0.15 ± 0.05	0.25 ± 0.10 [*, ††]	0.27 ± 0.15 [*, ††]	0.13 ± 0.03	
p	0.089	0.001	0.023	0.152	
EDV (ml)					
Baseline	0.27 ± 0.05	0.27 ± 0.07	0.32 ± 0.07	0.31 ± 0.04	0.32 ± 0.04
4 weeks	0.34 ± 0.08	0.43 ± 0.08 [*, ††]	0.41 ± 0.13	0.34 ± 0.05	
p	0.017	0.001	0.054	0.192	
ESV (ml)					
Baseline	0.11 ± 0.03	0.11 ± 0.02	0.13 ± 0.04	0.12 ± 0.03	0.11 ± 0.02
4 weeks	0.15 ± 0.05	0.23 ± 0.11 [*, ††]	0.23 ± 0.11 [*, ††]	0.13 ± 0.02	
p	0.014	0.003	0.018	0.207	
FS (%)					
Baseline	35.74 ± 4.34	32.92 ± 10.41	34.62 ± 4.54	3.02 ± 6.70	34.08 ± 4.16
4 weeks	32.89 ± 7.96	26.10 ± 11.76	28.01 ± 8.15	30.49 ± 8.87	
p	0.337	0.005	0.026	0.368	
FAC (%)					
Baseline	57.55 ± 11.70	64.62 ± 10.40	55.65 ± 12.80	62.06 ± 8.23	0.70 ± 0.07
4 weeks	50.30 ± 32.94	42.13 ± 20.17 [*, ††]	49.05 ± 16.06 [*]	60.20 ± 8.58	
p	0.454	0.008	0.149	0.627	
EF (%)					
Baseline	59.22 ± 6.88	57.69 ± 4.58	59.71 ± 5.39	61.67 ± 6.87	65.21 ± 4.28
4 weeks	56.07 ± 9.86	47.57 ± 16.44 [††]	47.46 ± 13.65 [††]	59.61 ± 5.86	
p	0.208	0.026	0.013	0.590	
SV (ml)					
Baseline	0.18 ± 0.07	0.15 ± 0.05	0.19 ± 0.04	0.19 ± 0.03	0.36 ± 0.09
4 weeks	0.20 ± 0.09	0.20 ± 0.06	0.19 ± 0.07	0.20 ± 0.04	
p	0.644	0.034	0.968	0.702	

LVIDd – left ventricular diameter diastolic; LVIDs – left ventricular diameter systolic; LVAd – left ventricular area diastolic; LVAs – left ventricular area systolic; EDV – end diastolic volume; ESV – end systolic volume; FS – factional shortening; FAC – fractional area change; EF –

ejection fraction; SV – stroke volume. Values are represented as mean ± SD; p is the difference between baseline and 4 – week post-treatment measurements (paired t-test); * $p < 0.05$ vs. saline,

Table 3.2: Echocardiography functional study Continued

† $p < 0.05$ vs. PEG-ND, †† $p < 0.05$ vs. ECM, 2-way ANOVA. (ECM data was provided courtesy of Sonya Seif-Naraghi, Department of Bioengineering, University of California San Diego)

3.3.3 Cellular response to injection

Immunohistochemistry analysis was performed to assess the effect of biomaterial injection on neovascularization in the infarct area. There was a significant increase in the saline injected hearts compared to PEG-ND injected animals for vessel diameters greater than 10 μm and ranging between 10 μm and 25 μm in the infarct region (Figure 3.5). There were no differences in myofibroblast density among the PEG-ND, PEG-D and saline injected animals (Figure 3.6). The immune response to injection was assessed by quantification of macrophage density within the infarcted region of the heart. The density of CD 68+ macrophages (M0) was the same among all groups, thus indicating that total macrophage infiltration in the infarcted region was the same. The density of CD 163+ macrophages (M2) was significantly greater in the PEG-ND hearts compared to the PEG-D. However, assessment of the M2/M0 ratio resulted in PEG-ND hearts having a higher ratio than PEG-D and saline hearts. Thus, these results indicate a higher ratio of remodeling associated macrophages (M2) compared to total macrophages in the PEG-ND hearts (Figure 3.7).
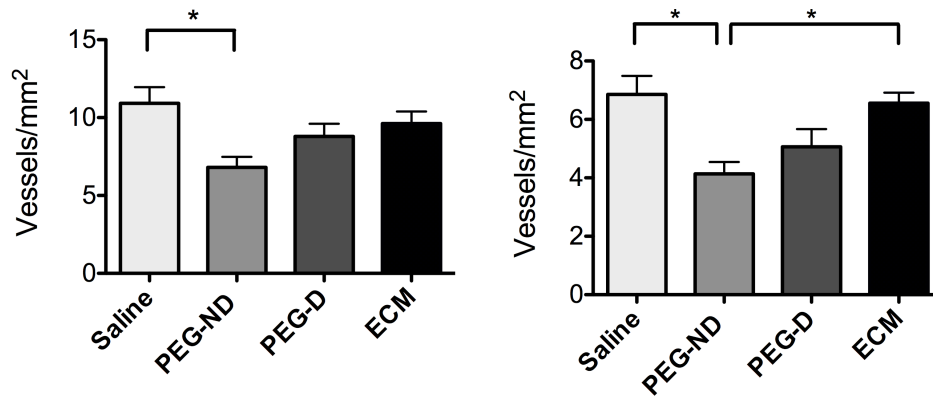
Figure 3.5: Arteriole density post-treatment.
(Left) Arteriole density (vessel diameter between 10 µm and 100 µm) and (Right) Arteriole density (vessel diameter between 10 µm and 25 µm) 5 weeks after MI. There is significantly reduced neovascularization in the PEG-ND injected animals. $P < 0.05$. (ECM data was provided courtesy of Sonya Seif-Naraghi, Department of Bioengineering, University of California San Diego)
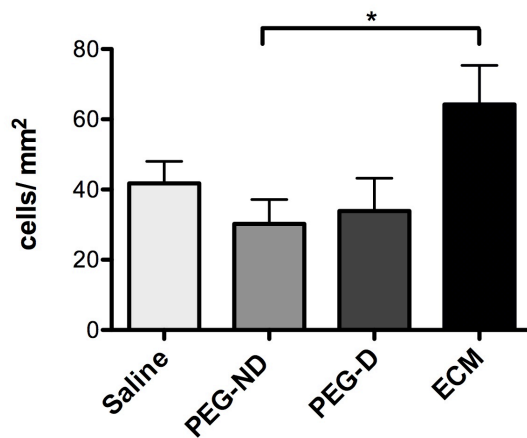
Figure 3.6: Myofibroblast density post-treatment.
Myofibroblast density in the infarct 5 weeks after MI. There is significantly reduced myofibroblast density in the PEG-ND injected animals. $P < 0.05$. (ECM data was provided courtesy of Sonya Seif-Naraghi, Department of Bioengineering, University of California San Diego)
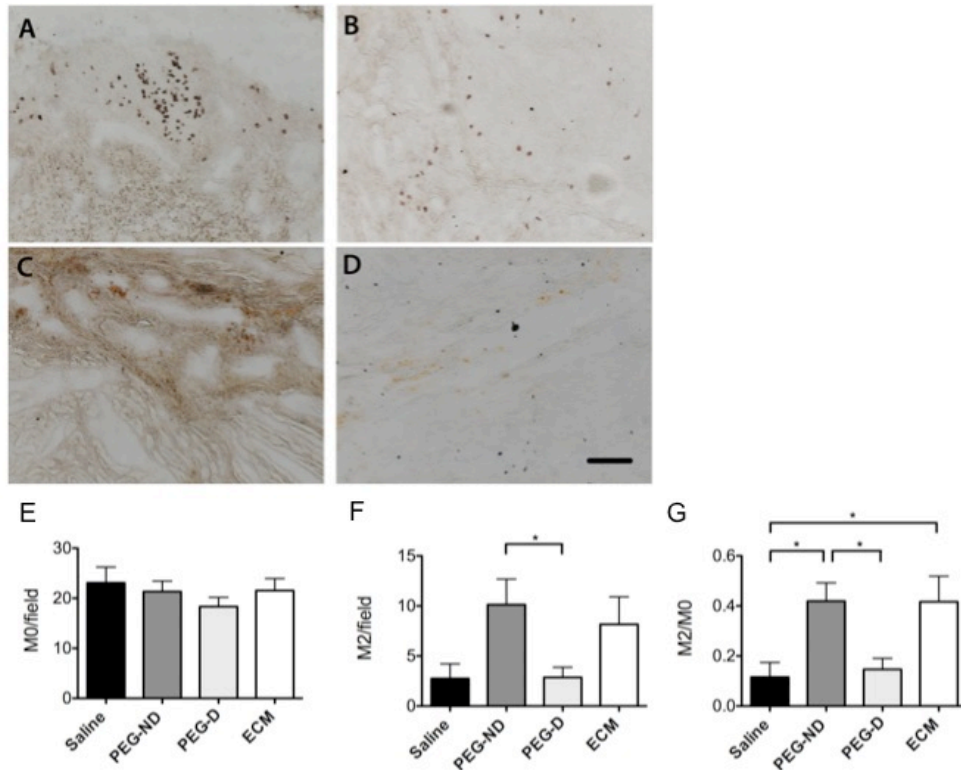
Figure 3.7: Macrophage response.
Representative photomicrographs of CD 163+ (M2) macrophages (A) PEG-ND, (B) PEG-D, (C) ECM, (D) saline. Total M0 macrophage density remained the same among injection groups (E). The density of M2 macrophages was significantly greater in the PEG-ND hearts compared to the PEG-D hearts (F). The ratio of M2/M0 was greater in the PEG-ND group compared to PEG-D and saline groups. Additionally, ECM injection demonstrated a greater M2/M0 compared to saline injection in the infarct. $P < 0.05$. (ECM data was provided courtesy of Sonya Seif-Naraghi, Department of Bioengineering, University of California San Diego)

3.3.4 Comparison to biologically active ECM material

At the time of this study, a biologically active ECM derived hydrogel prepared from decellularized porcine pericardium was injected into 8 rat MIs with subsequent analysis done with identical study parameters as those used for the PEG-ND, PEG-D and saline groups. (Data provided courtesy of Sonya Seif-Naraghi, Department of Bioengineering, University of California San Diego).

This data is shown here as a comparison between a bioactive material and the non-bioactive PEG materials. Injection of the bioactive ECM material demonstrated a decrease in wall thickness compared to the PEG injected groups and the saline. However, there was a preservation of LV geometry in terms of LV area and diameter in the ECM injected hearts (5 weeks post-MI) while there was increased diastolic area and systolic diameter in the PEG and saline groups (Table 3.1). On a cellular level, injection of a bioactive material resulted in an increase in neovascularization as well as an increase in myofibroblast density compared to PEG-ND injected hearts. There was also an increased ratio of M2/M0 similar to the PEG-ND hearts. (Figure 3.5, Figure 3.6 and Figure 3.7).

3.4 Discussion

Injectable biomaterial treatments are a promising approach for the mitigation of LV remodeling post-MI with a few materials now in large animal preclinical trials [9] and one material in clinical trials [138]. As these become more accessible it is important to understand the mechanism of action by which these materials induce the beneficial effects so as to tailor existing biomaterials and design more effective therapies. Previously, we have shown that the increase in wall thickness by injection of a synthetic non-degradable biomaterial in a rat total occlusion MI model was capable of creating a permanent increase in wall thickness, however that increase in wall thickness alone was insufficient to prevent negative LV remodeling and a decline in cardiac function (Chapter 2).

These results lead to the premise that passive structural support of the vulnerable LV wall was likely not the mechanism by which these biomaterials were providing benefit. It is likely other factors such as the inherent bioactivity or the degradability of biomaterials that possibly allowed for cell infiltration. Herein, we studied the effect of biomaterial degradation on the LV remodeling and cardiac function post-MI. Injection of a degradable, non-bioactive material (PEG-D) in an occlusion-reperfusion MI model led to a decline in function comparable to that of a similar material that was non-degradable (PEG-ND). In addition, the lack of improvement after synthetic non-degradable material injection seen in a permanent occlusion MI model [72] was reaffirmed in this occlusion-reperfusion model.

PEG was utilized in this study due to the tunability of its chemical and physical properties. Both PEG-D and PEG-ND are non-bioactive [106-109] as the hydrophilicity of the polymer prevents protein adsorption and hence cell adhesion. PEG-D contains a hydrolysable ester linkage allowing for the controlled degradation (~ 4.5 weeks) of the PEG-D based hydrogel *in vivo*, similar to the degradation time of other commonly injected materials.

Injection of a bioactive ECM based material led to preserved LV geometry compared to the PEG and saline injected hearts, however based on histological analysis, the ECM injected hearts had a thinner wall compared to the other groups. This apparent paradox may be explained by potential diastolic dysfunction in the PEG and saline hearts, preventing the complete relaxation and

arrest of the hearts in diastole when compared to the ECM injected hearts, and therefore resulting in a perceived thickening of the wall due to incomplete relaxation. The beneficial effects on LV geometry and cellular response with the biologically active material is likely due to the inherent bioactivity of the ECM and the ability for cellular recruitment due to the unique biochemical composition and degradation products [7,62].

Along with biologically derived materials, several synthetic degradable materials have been injected for the treatment of MI. For example a MMP-degradable PEG gel (6 week degradation) has been shown to enhance cardiac function [73]. This effect could be due to increased cell infiltration in the gel. The gels were designed to be bioactive and contain collagen-derived MMP-sensitive crosslinking peptides that allow fibroblasts to migrate in by integrin and MMP-dependent mechanisms [139]. One explanation for the lack of improvement seen with the degradable PEG based polymer in this study may be the inability for the material to facilitate adequate cellular recruitment. There was a decline in wall thickness in the PEG-D injected hearts, indicating that cellular infiltration could not occur at a level sufficient for preservation of wall thickness. This may be attributed to the non-bioactive properties of polymer.

PEG is well characterized as a non-fouling surface, resisting protein adhesion [140]. However, protein adsorption may be an important mechanism by which biomaterial aid in cardiac repair. Protein adsorption can lead to integrin binding allowing for activation of cellular responses such as cell infiltration and

differentiation. These cells could lead to paracrine effects from cell-secreted molecules such as cytokines, chemokines and growth factors which can influence negative LV remodeling by increasing cell survival and differentiation, cell recruitment, tissue contractility, and neovascularization [141-143]. Furthermore, many of the biologically derived materials contain ECM components. These ECM components are composed of proteins and glycosaminoglycans (GAGs) that can bind and sequester growth factors [144]. In addition to the biomaterials themselves, the degradation products of biologically derived materials may influence cell recruitment; for example, fibrin is thought to have angiogenic degradation products [92]. This can further cause a signaling cascade that recruits other cell types to the biomaterial and hence the MI site as well. It is likely this complex bioactive process that mediates LV remodeling potentially leading to the ability of biomaterials to induce improvement in cardiac function and LV remodeling.

The arteriole density was statistically lower in the PEG-ND hearts and numerically lower in the PEG-D compared to the saline and ECM injected hearts. This lack of vessel formation could be due to the density of the PEG material that could serve as an impediment to vascular cell infiltration. In a study by Dai et al., injection of collagen increased infarct thickness, and stroke volume and EF compared to the saline control. Nonetheless, there was no neovascularization in the infarct [55]. This was thought to be due to the high concentration of collagen (65 mg/ml) [145]. However, another report demonstrates improved angiogenesis upon injection of collagen at a concentration of 1 mg/ml [53]. The higher concentration of

collagen likely forms a dense network that does not facilitate cell penetration into the material. The PEG hydrogels in this study were injected at a concentration of 100 mg/ml, which may have contributed to the lack of neovascularization. Perhaps, injecting a material at a lower concentration will facilitate improvement by providing a less dense structure and hence larger pore sizes that may be conducive for cell migration.

Though macrophage analysis resulted in a similar total macrophage (M0) response among all groups, the ratio of M2/M0 was higher in the non-degradable polymer and ECM group. This apparent discrepancy in results is likely attributed to different pathways of activation for the M2 macrophages. Macrophages have been shown to polarize into two different phenotypes – M1 and M2 [146]. M2 macrophages are traditionally anti-inflammatory and encourage tissue repair, regeneration and beneficial remodeling [146]. It is likely that the M2 response in the ECM injected hearts leads to beneficial remodeling assisting in the improved cardiac outcomes [147-149]. M2 macrophage activation is known to be stimulated by IL-4 and IL-13 [150]. However, it was recently shown that IL-4 is linked to increased cardiac fibrosis [151]. The PEG-ND injected hearts had a larger fibrotic scar area compared to the other groups. One explanation for the increased M2 expression in the PEG-ND hearts may be potentially elevated levels of IL-4 due to the presence of increased fibrosis in the hearts causing activation of the M2 macrophages. In the PEG-D and saline injected hearts the M2/M0 ratio is lower, indicating that there is a larger M1 response. The M1 macrophage phenotype is

pro-inflammatory, cytotoxic and associated with chronic inflammation [146], which elucidate the negative outcomes in the PEG-D and saline groups.

In this study an occlusion-reperfusion technique was used to generate an infarction in a rat model. The presented work evaluates the effects of material degradation on global cardiac function and cellular response. Hence, it was imperative to utilize a model that had viable myocardium within the vicinity of the infarct. This model has been widely used and has demonstrated the ability for cell infiltration with many biopolymers [53,100,152]. In addition, occlusion-reperfusion is a more clinically relevant model for acute MI patients who are increasingly receiving revascularization therapies. Though the permanent occlusion model is more commonly used, it generates large transmural infarctions with very little myocardial salvage. In a previous study a non-degradable PEG polymer was injected in a total occlusion model [72] and in the presented work a similar non-degradable PEG polymer was injected in a occlusion-reperfusion model. Both studies showed a similar worsening of function, however it may still be interesting to study the effect of a degradable PEG in the total occlusion model.

Herein, we selected the PEG-D material because of its ~5 week degradation *in vivo*. Currently injected biomaterials that have shown beneficial effects on LV remodeling degrade on a timescale of 1 to 8 weeks. While this study provides valuable information of the effect of the degradability on cardiac function, a study injecting multiple materials of different degradation times may

provide valuable information. Also the injection of biomaterials may have a transient beneficial effect. Dobner et al. showed that injection of a PEG-based material leads to improved LV geometry at 4 weeks but at 13 weeks that effect was diminished [71]. Thus, timing of functional assessment and biomaterial degradation could play a role in the extent of post-treatment improvement.

In conclusion, this work establishes that injection of a synthetic, non-bioactive degradable polymer is insufficient to improve cardiac function and adverse LV remodeling after an MI. It is likely that the capability for protein adhesion is an important characteristic of biomaterials that allow for cellular adhesion, recruitment, and differentiation that can thus improve functional outcomes. As a result, inherent bioactivity and ability for cell and protein adhesion have been identified as important considerations during the design, development and application of biomaterials for the treatment of MI.

CHAPTER FOUR:

Hydrogel injection in myocardium results in a potential substrate for arrhythmias

4.1 Introduction

With the promise of injectable materials, it is important to fully understand the mechanisms by which these materials affect the underlying tissue and the impact of these materials on not only treatment of the pathological condition, but also on cardiac arrhythmogenesis.

Previous studies have shown injection of certain cell types disturb normal electrical propagation through the tissue and increase vulnerability to dangerous ventricular arrhythmias [153-155]. Along similar lines, injection of a material in the myocardium could cause conduction abnormalities and alter propagation; hence serving as a potential substrate to arrhythmia and ultimately a hazard to patient safety. However to date, studies aimed at understanding the effect of biomaterial injection on cardiac electrophysiology and arrhythmogenesis, an important component to the safety of such therapies, are lacking.

A variety of both biologically derived and synthetic biomaterials have been injected into infarcted tissue as a potential therapy for MI. There is wide heterogeneity in both the spread and site of delivery of these biomaterials. Many researchers believe injection of a biomaterial in the infarcted region of the myocardium may be advantageous by augmenting LV wall mechanics and promoting cellular migration into the region, on the other hand some postulate that injection into the viable border zone may improve myocardial salvage and prevent infarct expansion. One concern is that the presence of the material in

viable tissue may make that region vulnerable to alterations in electrical propagation. In addition to location of injection, distribution of the injection may also play a role in changing the conductivity of the extracellular environment and hence influence the electrophysiological properties of the underlying tissue. Moreover, different materials demonstrate varying degrees of spread through the myocardium ranging from formation of a bulk to a more disperse spread through the tissue [64,68,92].

Optical mapping is widely established as a robust technique for the detection, visualization and quantification of electrophysiological changes in cardiac tissue [156]. This technology has been recently utilized for the assessment of changes in electrophysiology and potential arrhythmogenesis after infarction [157,158] and cellular transplantation at the site of infarction [98,159]. Herein, we utilize optical mapping as a tool to assess the effects of injection of a bulk hydrogel as well as a disperse material (microbeads) on regional epicardial activation and recovery patterns in viable myocardium to assess the potential of these material injections on becoming substrates for arrhythmias.

4.2 Methods

4.2.1 Preparation of injectable materials

Hydrogels were prepared as previously described [72]. Briefly, poly(ethylene glycol) PEG hydrogels were prepared by mixing solutions at 100 mg/ml of 4-arm polyethylene glycol-amide-succinimidyl glutarate (PEG-ND) (JenKem, MW

20,000) and 1mg/ml trilysine (Sigma-Aldrich) to create PEG hydrogels at room temperature by chemical crosslinking. Both the solutions were mixed together and injected into the LV myocardium prior to gelation. Polymer microbeads were fabricated as follows. Acetalated dextran (AcDex) was prepared as described previously [160,161]. In order to visualize the microbead distribution after injection, AcDex was labeled with Alexa594 fluorophore (AF594). AcDex (60% cyclic acetals, 500 mg, 0.05 mmol) was dissolved in dry DMSO (Acros Organics; 12 ml). Triethylamine (Sigma; 100 μl, 0.717 mmol) was added to the DMSO/AcDex solution. Next, dichloromethane (DCM, Fischer Scientific; 2 ml, 31.3 mmol) containing AF594 carboxylic acid succinimidyl ester (Life Technologies; 1mg, 0.001mmol) was added. The solution was left stirring at room temperature for four days. DCM was evaporated using a rotary evaporator. The precipitate was dissolved in 10 ml tetrahydrofuran (THF). The AF594/THF solution was combined with water (pH 8.0) in a 1:20 ratio to precipitate the labeled polymer. The water/THF mixture was centrifuged at 5000 x g for 5 minutes. The supernatant was removed and residual THF was removed by rotary evaporation. The remaining solid was frozen and lyophilized to yield a solid pellet with faint purple color.

Microbeads were prepared using an oil-in-water emulsion procedure. Briefly, 25 mg of AcDex (labeled or unlabeled) was dissolved in 1ml of DCM. The dissolved AcDex was added to 50 ml of phosphate buffer (pH 7.4) containing 1% Poly Vinyl Alcohol (Sigma). The mixture was stirred at 1000 rpm for 10

minutes to prepare an emulsion. The emulsion was stirred at low speed under vacuum for 30 minutes to evaporate DCM. The resulting microbeads were pelleted by centrifugation and then washed with phosphate buffer (pH 8.0; 2 x 15 ml) and then ddH$_2$0 (3 x 15ml). Microbeads were frozen and lyophilized. Microbead size and morphology were evaluated with a Beckman Coulter Multisizer 4 and Agilent 8500 FE-SEM, respectively. Prior to injection, microbeads were suspended in phosphate buffer (pH 7.4) at a concentration of 20 mg/ml.

4.2.2 *In vivo* hemodynamic measurements and injection surgery

Female Sprague Dawley rats were anesthetized using 5% isoflurane, intubated and maintained at 2.5% isoflurane for the surgery procedure. The animals were ventilated using a respirator at 75 breaths/minute. The right carotid artery was carefully isolated and a pressure transducer (Millar) was inserted in through the carotid artery and advanced into the left ventricle. The isoflourane was reduced to 1% and the ECG and LV pressures were monitored and recorded. End diastolic pressure (EDP) was defined as the LV pressure at the peak of the QRS complex while peak systolic pressure (PSP) was established as the maximum LV pressure. All pressure measurements were averaged over 10 beats in the cardiac cycle. Immediately after pressure measurements, the heart was exposed using a left anterior thoracotomy and injected with either 150 μl of the hydrogel, microbeads or saline using a 27 G needle into LV free wall or not

injected, as a sham group. Isofluorane was maintained at 2.5% during the injection procedure. Presence of the injection was verified by temporary discoloration of the tissue. Hemodynamic parameters were measured after injection as was done at baseline.

4.2.3 Optical mapping of the polymer injection in Langendorff-perfused rat heart

Immediately after post-injection hemodynamic measurements, the hearts were excised and arrested using a solution containing 25 mM NaHCO$_3$, 2 mM CaCl$_2$, 5 mM Dextrose, 2.7 mM MgSO$_4$, 22.8 mM KCl, 121.7 mM NaCl, 20 mM 2,3 butanedione monoxime. The aorta of the heart was cannulated and attached to a Langendorff apparatus. The hearts were then retograde perfused with a Tyrode's solution (25 mM NaHCO$_3$, 2 mM CaCl$_2$, 5 mM Dextrose, 2.7 mM MgSO$_4$, 4.8 mM KCl, 121.7 mM NaCl, 10 mM Blebbistatin) at 37º C in a custom designed optical mapping chamber. A constant pressure of 70 mmHg was maintained and the flow rate was monitored. Blebbistatin was used as an electromechanical decoupler as previously shown to minimize motion artifact [162].

The heart was stained with the voltage sensitive fluorescent dye di-4-ANEPPS that was dissolved in dimethysulfoxide (DMSO) and diluted to 5.2 mM with Tyrode's solution. A 10 ml bolus of this solution was injected into the perfusion line. The LV free wall was imaged with a high-speed CMOS camera (MiCAM Ultima L, Brainvision) using a custom-built tandem lens imaging

system, with an objective lens of 0.5X and imaging lens of 1X (Leica planapo objective). Imaging was done with a spatial and temporal resolution of 100 x 100 pixels at 0.2 mm x 0.2 mm per pixel, and a frame rate of 1000 frames per second. The dye-stained LV epicardial surface was excited by an LED lamp (LEDtronics) at 470 nm (excitation of the LED lamps) and the emitted fluorescence was collected and filtered with a long-pass filter >610 nm (Figure 4.1). The images were collected at intrinsic cardiac rhythm.
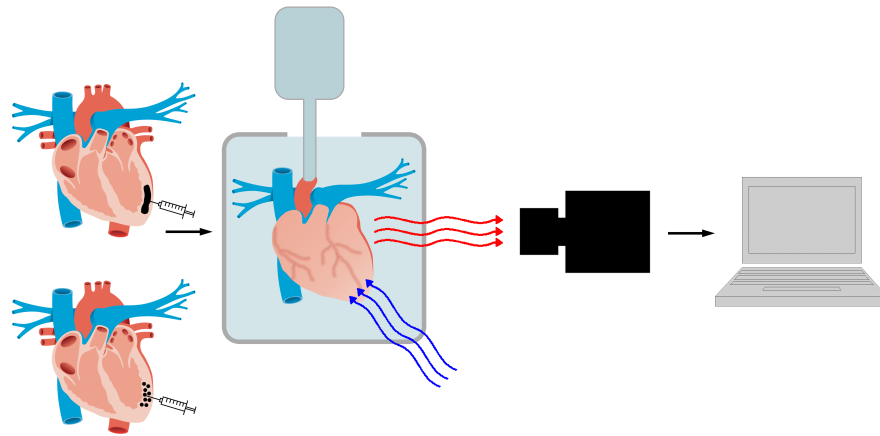
Figure 4.1: Schematic of experimental procedure
The hearts injected with the hydrogel or microbeads are depicted, followed by the optical mapping setup. The heart is excised and the aorta is cannulated for perfusion of the tissue with Tyrodes solution, allowing the heart to remain viable *ex-vivo*. A voltage sensitive dye (di-4-ANNEPS) is perfused through the coronaries. A LED light excites the dye at 470 nm (blue arrows) and the emitted fluorescence is collected at a wavelength greater than 610 nm (red arrows). The incident fluorescent signal is captured by a high-speed camera (1000 frames/second) and then computational techniques are used to analyze the data.

4.2.4 Data Analysis

Optical signals were imported into Matlab and analyzed using custom software as previously described [163]. Briefly, activation time was identified at each pixel as the time of maximum rate of change of fluorescence for the action

potential upstroke for each beat $(dF/dt)_{max}$. To calculate the time of repolarization, the time at which the action potential recovered to 20%, 50%, and 80% of the peak value were determined. The action potential duration (APD) at 20%, 50%, and 80% were calculated as the difference between repolarization time at the respective level and activation time of the action potential. The dispersion in APD and repolarization times was calculated as the difference between the maximum and minimum APD or repolarization time over the LV epicardium in the field of view respectively.

4.2.5 Histology

After the completion of the optical mapping experiments, the heart was removed off the cannula and the region of the LV epicardium was marked using tissue paint. The hearts were then fresh frozen in Tissue-Tek O.C.T. freezing compound and were sectioned into 10 μm slices with slides taken every 0.4 mm. The slides were stained with hematoxylin and eosin (H&E) to visualize the polymer injection and determine polymer spread. Images were taken using a Carl Zeiss Observer D.1 and analyzed using Axiovision software.

4.2.6 Statistical Analysis

A one-way analysis of variance (ANOVA) test with a Newman-Keuls post-hoc analysis was used to detect differences among groups for the pressure and activation time measurements. A two-way ANOVA test with a Bonferroni

post-hoc analysis was used to detect differences in dispersion of APD and repolarization at 20%, 50% and 80% levels. All measurements were reported mean ± SEM, unless otherwise specified. Significance was accepted at $p < 0.05$.

4.3 Results

4.3.1 Hemodynamic measurements

Hemodynamic measurements were performed at baseline to ensure normal cardiac behavior and also as a comparison for post-injection measurements. The average baseline LV EDP and PSP in the rat hearts included in the study was 8.1 ± 1 mmHg and 84.0 ± 2.7 mmHg respectively, signifying normal cardiac function. 22 animals underwent either saline (n = 5), microbeads (n = 6) or hydrogel (n = 6) injection or were a no injection control (n = 5). 100% of the animals survived the injection surgery. Measurement of the hemodynamic properties acutely after injection demonstrated no statistical differences in LV EDP and PSP, indicating no acute changes in hemodynamic parameters upon injection of the biomaterials (Table 4.1).

Table 4.1: Hemodynamic parameters

	Baseline		Post-injection	
	EDP (mmHg)	PSP (mmHg)	EDP (mmHg)	PSP (mmHg)
Bulk Polymer	8.5 ± 1.7	88.4 ± 2.0	8.0 ± 2.0	89.6 ± 3.3
Microbeads	7.1 ± 2.5	73.8 ± 7.5	7.2 ± 2.8	82.7 ± 5.2
Saline	7.6 ± 1.2	89.7 ± 3.1	5.7 ± 1.2	87.9 ± 3.9
No injection	9.8 ± 1.5	85.4 ± 5.6	9.0 ± 2.7	84.5 ± 6.0

4.3.2 Optical mapping and histological analysis

Immediately after post-injection hemodynamic measurements the hearts were excised and arrested. Electrical propagation in the isolated rat heart was studied using a Langendorff, aorta-perfused setup. Fluorescent images of epicardial surface of the heart were obtained to verify the perfusion of the dye over the entire epicardium (Figure 4.2 A) Histological analysis was performed upon completion of the optical mapping study to verify the presence and distribution of material in the injection region (Figure 4.2 B-E). In Figure 4.2 E, the hydrogel injection region is clearly visible and the hydrogel forms a bolus in LV free wall myocardium. Alternatively, the inset in Figure 4.2 D depicts the fluorescently labeled microparticles distributed diffusely through the tissue.

Figure 4.2: Histological analysis.
(A) Representative fluorescent image of the di-4-ANNEPS perfused hydrogel injected heart. Note: dye perfusion over the entire epicardial surface. Histological assessment of no-injection (B) and saline (C), microbead (D) and hydrogel (E) injection after optical mapping. Representative slides stained with H&E. The region of bulk polymer in the myocardium is delineated by a dotted line and asterisk. Inset in (D) is a 100X magnification fluorescent image of the microbeads localized in the tissue (scale bar 200 μm). All other photomicrographs are taken at 10X and scale bar is 2mm.

4.3.3 Altered action potential propagation

To determine the electrophysiological impact of the polymer injections, action potential propagation through the tissue was studied. Irregular propagation patterns can indicate a conduction block in the underlying tissue that could potentially cause delayed conduction in the myocardium and moreover, act as a substrate for arrhythmias. To study this, action potentials were obtained by observing the change in fluorescence of the voltage sensitive dye as has been previously shown [163]. A dynamic display of the changes in fluorescence intensity with time was viewed to determine any alterations in action potential propagation patterns and directionality due to injection of a biomaterial. Presence of a bulk hydrogel created local disturbances leading to irregularities in direction of propagation as well as overall slowing of activation compared to the microbead or saline injected animals or hearts with no injection at all.

4.3.4 Polymer injection leads to activation delays

To better understand the alterations in action potential propagation seen due to the presence of the bulk material, activation maps were constructed to depict impulse propagation. Activation time at each pixel was taken to be the time of maximum change in fluorescent signal (dF/dt). Representative color maps indicate that activation times were prolonged in the hydrogel injected hearts with clear activation delays in the region of material injection (Figure 4.3 A - D). Injection of the bulk polymer led to significant increase in total LV epicardial

activation time (mean ± SD), 11.3 ± 4.4 ms compared to microbeads 5.9 ± 3.7 ms, saline 4.9 ± 1.3 ms and no-injection 5.0 ± 2.0 ms (p < 0.05), indicating that the bulk hydrogel served as a barrier to impulse conduction by slowing or blocking action potential propagation (Figure 4.3 E).
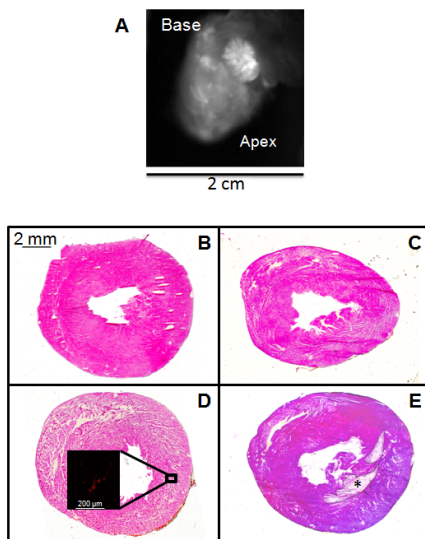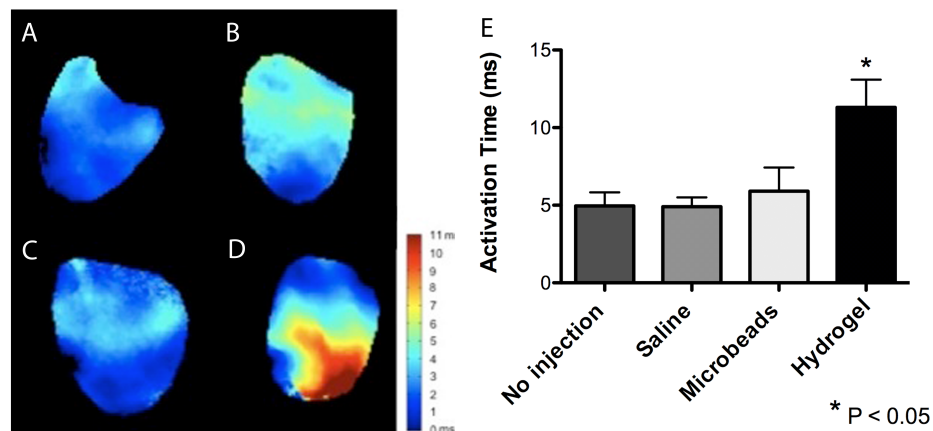

Figure 4.3: Activation time.
(A) Representative fluorescent image of the di-4-ANNEPS perfused hydrogel injected heart. Note: dye perfusion over the entire epicardial surface. Histological assessment of no-injection (B) and saline (C), microbead (D) and hydrogel (E) injection after optical mapping. Representative slides stained with H&E. The region of bulk polymer in the myocardium is delineated by a dotted line and asterisk. Inset in (D) is a 100X magnification fluorescent image of the microbeads localized in the tissue (scale bar 200 μm). All other photomicrographs are taken at 10X and scale bar is 2mm.

4.3.5 Changes in other electrophysiological parameters

Variation in action potential duration (APD) and repolarization can increase the likelihood for reentrant arrhythmias by creating local disturbances in the tissue [164]. Measurements of action potential characteristics such as APD at 20%, 50% and 80% repolarization levels demonstrate no significant changes in APD_{20}, APD_{50} and APD_{80} by the injection of the bulk or disperse biomaterial (Figure 4.4 A - C). However, there is a significantly greater dispersion in APD_{80}

and a trend for increased dispersion at APD_{20} and APD_{50} (Figure 4.4 D - F) in the hydrogel injected group compared to the microbeads, saline, and no injection groups. Similar results were seen for dispersion of repolarization as well (Figure 4.5). This indicates that the bulk material may create heterogeneities in the underlying tissue causing a greater variation in action potential characteristics. The slowing of activation as well as the greater dispersity in action potential duration and repolarization may create an underlying substrate for arrhythmia by increasing ventricular electrical irritability when material is injected in a bulk form, however when injected in a more disperse form that spreads through the tissue, such as with microbeads, the deleterious effects are mitigated.
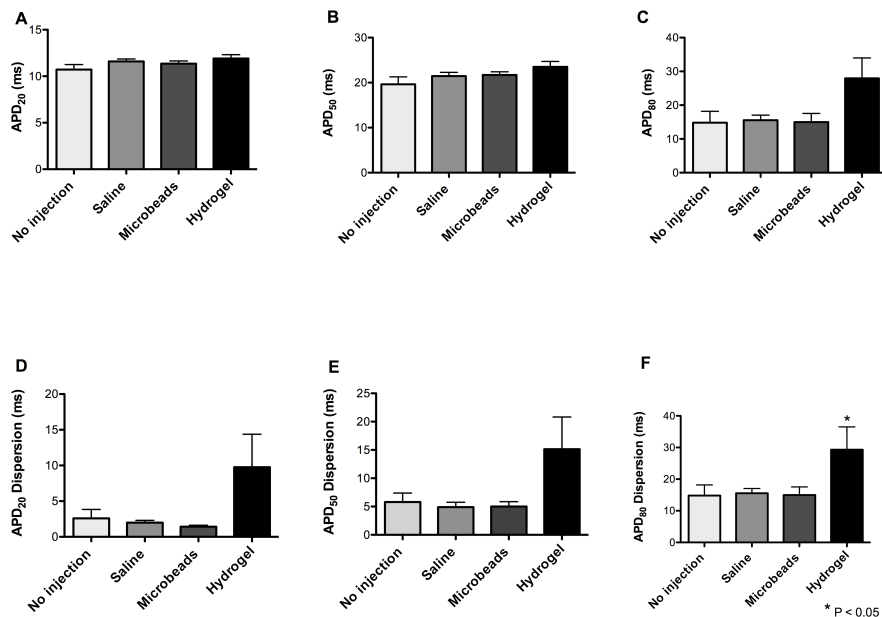
Figure 4.4: Action potential duration.
APD at 20% (A), 50% (B) and 80% (C) repolarization and dispersion of APD at 20% (D), 50% (E) and 80% (F) repolarization. Dispersion of APD_{80} is significantly greater in the bulk hydrogel injected group compared to all other groups. *P < 0.05.
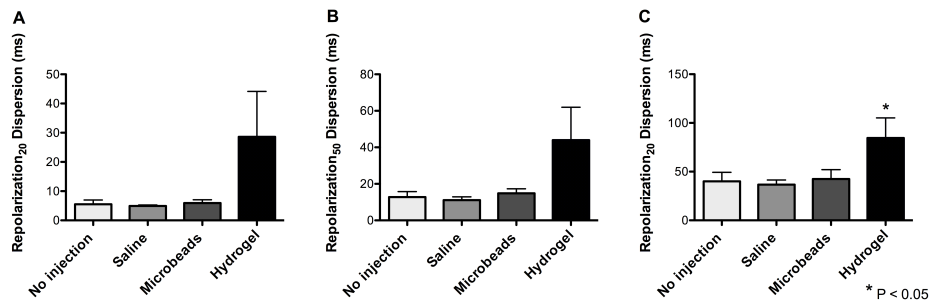
Figure 4.5: Dispersion of repolarization.
Dispersion of repolarization at 20% (A), 50% (B) and 80% (C). Dispersion of repolarization at is significantly greater in the bulk hydrogel injected group compared to all other groups. *P < 0.05.

4.4 Discussion

With the rapid increase in potential injectable biomaterial therapies for myocardial repair after infarction and HF, the question of safety of biomaterial injection is an important issue and pre-requisite to clinical translation. In this study the important but overlooked issue of electrophysiological impact of material injection during these procedures was studied. Utilizing optical mapping, we were able to assess the effect of intramyocardial injection on the global electrophysiological parameters – activation time, APD, and repolarization. Most importantly, we discovered that injection of a bulk hydrogel leads to significant activation delays as well as greater variation in APD and repolarization times. In contrast, injection of a biomaterial, which has a more disperse spread in the tissue, such as in the form of microbeads, does not alter the action potential characteristics.

A potential mechanism by which the injection of the hydrogel leads to such alterations may be due to the presence of the bolus of material functioning as

a conduction block. As seen in the case of many biomaterial injections in LV tissue, the injection of the PEG polymer localized to the site of injection, thus forming a discrete region in the myocardium with different electrical properties. This material likely serves as an obstacle to conduction through the myocardium that may result in an overall slowing of activation time. It is now widely accepted that cardiac electrical conduction is a function of not only the cellular conductivity but also the conductivity of the extracellular space [165,166]. While the presence of the material may not change the intracellular properties, it may affect the local extracellular conductivity as well as potentially disrupt gap junctions between the conductive cardiomyocytes. Disturbance in gap junctions has been associated with induction of harmful ventricular arrhythmias in small animal studies [167]. Thus injection of a bulk hydrogel could lead to the alterations and heterogeneity of action potential characteristics and moreover, increase the arrhythmogenicity of the tissue. However, injection of microbeads may not function as a conduction block due to their small size and greater spread through the tissue. As a result distribution of the biomaterial in the tissue may be an important factor to consider when designing injectable biomaterial therapies for MI.

In addition, controlling where biomaterials localize in the tissue is a challenge. Materials of a wide range of viscosities and stiffnesses have been injected into the LV myocardium resulting in varying degrees of spread through the tissue. Injectable biomaterial treatments for MI therapy involve materials

utilizing a wide variety of gelation mechanisms. For example, materials such as alginate can crosslink in situ due to the presence of calcium ions in the infarct. This mechanism allows for a greater spread of the material in the tissue. One the other hand, materials such as fibrin are made of a two-component systems that gel immediately when the two components come in contact, resulting in less spread of the material. Furthermore, often injections targeted for the infarct can extend to the borderzone and healthy tissue where viable myocytes are present. Previous studies have showed that the infarct already has slowed or disturbed conduction[157], so injection of a biomaterial into the infarct may not cause conduction abnormalities superseding the effects of infarction injury . In a study by Singelyn et al., arrhythmogenesis was assessed in rat MI model 1 week after injection of a myocardial matrix hydrogel in the infarct region and there were no increases in incidences of arrhythmia [7]. Similar results were seen after both intracoronary and intramyocardial injection of different biomaterials in a porcine infarct [8,66]. On the other hand, the borderzone contains electrically viable and vulnerable tissue, so injection or spread of material into this region is a concern. Herein, we injected a biomaterial in viable myocardium to specifically understand the effect of material injection and spread on myocardial tissue containing viable myocytes (borderzone and healthy myocardium) and decouple any effects that could occur from the presence of the infarcted tissue.

Several biomaterials have been injected into infarcted myocardium in mainly rodent infarct models. While, most of these materials are injected in an acute or sub-acute infarct, there are limited studies that address application of these materials to chronic infarct [44]. In a chronic infarct where the remodeling cascade is largely completed, the electrophysiological properties of the tissue may be different than in the remodeling infarct where there may be clusters of viable myocytes. To date, there are only limited studies that have looked into the electrophysiological impact of material injection in the acute infarct and to the best of our knowledge there are no reports on the effect in the chronic infarct.

As was noted during evaluation of arrhythmogenesis due to cellular cardiomyoplasty, patients eligible for this therapy may already be at high risk for arrhythmias and may be fitted with an internal cardioverter defibrillator (ICD) [168]. As injectable biomaterial treatments progress to the clinic the patient demographic will have to be carefully selected so as to not increase the ventricular vulnerability above the baseline level, so that the risk of biomaterial injection on ventricular arrhythmia is outweighed by the beneficial improvement in cardiac function.

In this acute study, 150 µl injections were selected, as it is a common injection volume in rodent MI studies [9,44]. Though the volume of injection was maintained constant with both the material types, the concentration of polymer was different between both materials. Herein, we injected a PEG hydrogel with a polymer content of 100 mg/ml to create a gel with similar mechanical properties as other commonly injected material for biomaterial MI therapy [72]. Along the

same lines, typical microbead injection in the heart ranges between 10 - 20 mg/ml of microbeads; hence, we injected microbeads at a concentration at 20 mg/ml to mimic common concentrations for cardiac injection [169-171]. In addition, two different biomaterials were injected - PEG as a bulk hydrogel and acetalated dextran microbeads as a more distributed form of material, as these materials were well characterized in the laboratory. Nonetheless, as the material injected hearts were excised within one hour of injection, there is negligible immune response expected from the host tissue due to the presence of the biomaterial. At this acute time point the material functions mainly as a physical barrier and does not react with the tissue, therefore the differences in chemical properties of these materials should not affect the outcomes of this study. However, further studies aimed at assessing the effect of biomaterial injection at longer and more prolonged duration in both viable and infarcted myocardium would be of interest.

In conclusion, injection of a bulk hydrogel in myocardium may create a substrate for reentrant arrhythmia by causing activation delays and local heterogeneities in conductivity at the site of injection when compared to a more dispersed material, such as in the form of microbeads. While injection into the infarct may not be a concern given the already slowed or perturbed conduction, our results indicate that delivery of a bulk material into viable or border zone myocardium may have deleterious effects, establishing site of delivery and distribution of biomaterial in the tissue as important factors in the future use and development of biomaterial therapies for MI treatment.

Chapter 4, in full, is in submission as: Rane AR, Wright AT, Suarez SL, Zhang SX, Braden RL, Almutairi A, McCulloch AD, Christman KL. Hydrogel injection in myocardium results in a potential substrate for arrhythmias.

The author of this dissertation is one of the primary authors or co-author on all publications.

CHAPTER FIVE:

Summary and future work

5.1 Summary and conclusions

With MI affecting over one million Americans each year [172], there has been a push for the development of novel therapies for the treatment of MI, subsequent LV remodeling and HF. The field of biomaterials for treating MI has rapidly expanded over the past decade [5,9] and in particular, injectable biomaterials have been evaluated as potential minimally invasive therapies for MI and HF. Injection of materials such as collagen [55], alginate [8,44], fibrin [100], chitosan [48], small intestinal submucosa [59], myocardial matrix [7] and a few degradable synthetic materials [75,78,80] have shown therapeutic benefit in terms of global cardiac parameters such as improved or maintained LV geometry and EF. As these therapies show positive results along with potential for catheter delivery in some cases [7,8], many injectable materials are advancing to large animal pre-clinical models [8] and recently clinical trials [46]. With the promising results shown by these materials, this thesis aims at answering the important question of how injectable biomaterials influence cardiac function and LV remodeling post-MI.

PEG was chosen for the studies in this thesis due to the tunability of its properties and the fact that it is non-bioactive, consequently preventing protein and cell adhesion[173]. Thus, we were able to decouple the effects of mechanics from bioactivity, as well as tailor the mechanical and degradation properties to match those of commonly injected materials (Ch 2 & Ch 3). Injection of a non-degradable PEG demonstrated that passive structural intramyocardial support

(local wall thickening) by itself does not prevent negative LV remodeling or maintain cardiac function, suggesting that other mechanisms such as bioactivity and/or cell infiltration seen with degradable materials likely play a dominant role in the mitigation of LV remodeling and preservation of cardiac function (Ch 2).

As the next step, we studied whether cellular infiltration due to polymer degradation plays an important role in providing those beneficial effects. Assessment of cardiac function via echocardiography before and after treatment with both a degradable and non-degradable PEG demonstrated deterioration of function in both PEG polymer injected groups while cardiac function was largely preserved in the saline and the bioactive, degradable extracellular matrix (ECM) control. Additionally, the presence of the PEG material inhibited neovascularization and altered the macrophage response. The findings from this study indicate that degradability alone did not influence cardiac function and perhaps the ability for protein adsorption and cell adherence to a biomaterial may be an essential component of the many materials that have been studied for prevention of the structural and cellular changes associated with negative LV remodeling (Ch 3).

Along with understanding the important fundamental properties of the biomaterial itself, the effect of biomaterial injection and spread on cardiac arrhythmogenesis was studied. While MI itself is known to cause cardiac conduction abnormalities, limited studies have tested the implications of biomaterial injection on cardiac electrophysiology. Controlling the spread of an

injectable biomaterial is difficult, and often materials injected into the infarct can spread into the borderzone and healthy myocardium or alternatively, some materials are injected into the infarct borderzone by design. To investigate how the injection of materials in viable tissue affects cardiac conduction and arrhythmogenicity, optical mapping was utilized to study action potential propagation. Injection of a bulk hydrogel in the myocardium led to activation delays and greater dispersion of action potential duration and repolarization when compared to injection of microbeads (Ch 4). While delivery into the infarct may not be a concern given the already slowed or perturbed conduction, the results of this study indicate that delivery of a bulk material into viable or border zone myocardium may create a substrate for reentrant arrhythmia.

In conclusion, site of delivery and distribution of the biomaterial in the tissue, as well as ability of the material to promote protein adsorption and cell recruitment are likely important factors in the future use and development of biomaterial therapies for MI treatment.

5.2 Future considerations for biomaterial therapies

5.2.1 Cellularity and bioactivity of the scaffold

Both biological and synthetic biomaterials have been utilized for cellular or acellular cardiac applications. However, it is still unclear as to whether addition of cells causes functional improvement over the acellular scaffold. However, the majority of injectable therapies have shown similar improvements

in function and remodeling regardless of the cellularity of the construct. As highlighted in other sections of this thesis, both synthetic and biological materials have been tested as potential treatments for post-MI LV remodeling, with both materials showing promising outcomes. Biologically derived materials have the benefit of providing the adequate biochemical environment necessary for cellular recruitment to the damaged area and may better mimic the heart's extracellular environment. Then again, synthetic materials have the added benefit of material tunability to match complex cardiac mechanical properties and physical structure, such as pores.

5.2.2 Structural characteristics of the scaffold

The purpose of cardiac tissue engineering strategies for MI treatment is to mitigate tissue damage caused during infarction as well as curb processes such as infarct expansion and further deterioration of the injured myocardium. During the LV remodeling cascade there are structural changes in the LV such as wall thinning and collagen deposition leading to changes in stiffness of the infarct. With the different structural and mechanical changes in the infarct, stiffness of the biomaterial implant is an important consideration. In the case of injectable biomaterials, materials ranging from Pa range to the kPa range have been developed and tested. Berry et al. have shown the elastic modulus of the healthy myocardium is around 20 kPa [126], so it might be beneficial for biomaterials to have mechanical properties in this regime. On the other hand, individual ECM components lie in the 0.5 to 1 kPa range and may also have advantageous effects.

Ifkovits et al. studied the effect of changing material mechanics on cardiac function after MI. They demonstrated that injection of a stiffer material (43 kPa) close to the stiffness of infarcted tissue (55 kPa) [126], reduced scar size, but did not affect cardiac function [64]. Though ECM derived biomaterials have lower mechanical properties, techniques such as chemical crosslinking can be used to enhance the mechanical properties of the scaffold [174]. However, further studies investigating the effect of material mechanics on LV remodeling could provide some answers on how to best modulate mechanical properties of biomaterial treatments.

Another important characteristic of biomaterials is degradation rate. All of the bioactive and majority of the synthetic biomaterials used for cardiac tissue engineering applications are degradable in the range of 1 to 6 weeks [9]. Apt degradation of biomaterials may allow for timely cell infiltration allowing for repair of the infarct and salvage of the vulnerable borderzone area. These infiltrating cells may be valuable for increasing neovascularization and modulating the inflammatory response, with perhaps a greater M2 macrophage and T2 leukocyte response. In addition, the timely degradation may allow for transient changes in mechanical properties allowing for the stiffness to change as the material degrades. This may be beneficial in the remodeling infarct by initially providing support to the vulnerable tissue but then degrading over time to allow for cellular infiltration.

5.2.3 Time point of delivery and assessment

Currently, there is heterogeneity in time points for intervention with cardiac tissue engineering strategies. Intervention with injectable biomaterials in preclinical models is most commonly carried out immediately and 1 week after infarction. Immediately after infarction the myocardial wall is susceptible to rupture and hence this time point may not be clinically relevant. Most patches are implanted 2 to 4 weeks after the infarction [9], which is in the middle of the rat remodeling cascade that is largely complete by 5 weeks. The time point for delivery is an important criterion prior to human translation. As of today, it is still unclear as to whether these therapies should be used for acute or chronic MI patients. In most of the studies carried out to date, biomaterial therapies have been applied to acute or subacute infarcts and have shown beneficial effects. However, limited studies have applied these approaches to the chronic infarct and shown improvement in cardiac function [44]. Lately, there has been a greater push for reperfusion of MI patients, perhaps the most suitable time for delivery should mimic the time course of reperfusion. On the same token the impact of cardiac tissue engineering approaches have been assessed at various durations ranging with majority of studies evaluating effects at 4 weeks after biomaterial delivery. To better understand the efficacy of these approaches more studies at longer time points are needed. For example, injection of a synthetic polymer was shown to improve cardiac function at an early time point of 4 weeks but at later time point of 13 weeks that effect diminished [71].

5.3 Limitations and future work

There are some limitations in design of the studies presented in this dissertation, as well opportunities for future work.

In Chapter 2 and 3, two different MI models and imaging modalities were used in the studies making it difficult to compare results. As outlined in Chapter 3, the effect of materials with various *in vivo* degradation times at different time points (early/late MI) could provide added insight into the mechanism of action of these materials.

In Chapter 4, optical mapping is a surface technique and only allows for visualization of the epicardial surface. As a result, the study was performed on healthy rats. The use of optical mapping in an infarction model is challenging due to damaged vasculature in the infarct preventing staining of the epicardial surface. In addition, infarction itself is known to cause arrhythmia so it would be difficult to decouple effects due to infarction from those due to polymer injection. Programmed electrical stimulation is an alternative method to show arrhythmia inducibility after intra-infarct injection, however the sample size required made this study impractical. Also, as discussed in Chapter 4, two different biomaterials were injected – a PEG based polymer as the bulk hydrogel and a poly acetalated dextran as the microbeads. Moreover, two different concentrations of materials were used to mimic what was commonly injected. Future studies could be

performed in an MI model utilizing a single biomaterial in two different forms at the same concentration.

While this work, provides the initial groundwork for understanding how biomaterials affect cardiac function, there are many other possible properties of biomaterials that can be tailored potentially making them more suitable therapies for MI treatment, such as material porosity and mechanics as well as other factors discussed in section 5.2.

Chapter 5, in part, is in submission as: Rane AR, Watson J, Christman KL. Tissue engineering and applications for treatment of myocardial infarction.

The author of this dissertation is one of the primary authors or co-author on all publications.

References

1. Cleutjens JP, Kandala JC, Guarda E, Guntaka RV, Weber KT. Regulation of collagen degradation in the rat myocardium after infarction. Journal of Molecular and Cellular Cardiology 1995;27(6):1281-92.

2. Sutton MG, Sharpe N. Left ventricular remodeling after myocardial infarction: pathophysiology and therapy. Circulation 2000;101(25):2981-8.

3. Pfeffer MA. Left ventricular remodeling after acute myocardial infarction. Annu Rev Med 1995;46:455-66.

4. Whittaker P, Boughner DR, Kloner RA. Role of collagen in acute myocardial infarct expansion. Circulation 1991;84(5):2123-34.

5. Christman KL, Lee RJ. Biomaterials for the treatment of myocardial infarction. J Am Coll Cardiol 2006;48(5):907-13.

6. Reffelmann T, Kloner RA. Cellular cardiomyoplasty--cardiomyocytes, skeletal myoblasts, or stem cells for regenerating myocardium and treatment of heart failure? Cardiovasc Res 2003;58(2):358-68.

7. Singelyn JM, Sundaramurthy P, Johnson TD, Schup-Magoffin PJ, Hu DP, Faulk DM, Wang J, Mayle KM, Bartels K, Salvatore M and others. Catheter-deliverable hydrogel derived from decellularized ventricular extracellular matrix increases endogenous cardiomyocytes and preserves cardiac function post-myocardial infarction. J Am Coll Cardiol 2012;59(8):751-63.

8. Leor J, Tuvia S, Guetta V, Manczur F, Castel D, Willenz U, Petneházy O, Landa N, Feinberg MS, Konen E and others. Intracoronary injection of in situ forming alginate hydrogel reverses left ventricular remodeling after myocardial infarction in Swine. J Am Coll Cardiol 2009;54(11):1014-23.

9. Rane AA, Christman KL. Biomaterials for the treatment of myocardial infarction a 5-year update. J Am Coll Cardiol 2011;58(25):2615-29.

10. Li RK, Jia ZQ, Weisel RD, Mickle DA, Choi A, Yau TM. Survival and function of bioengineered cardiac grafts. Circulation 1999;100(19 Suppl):II63-9.

11. Leor J, Aboulafia-Etzion S, Dar A, Shapiro L, Barbash IM, Battler A, Granot Y, Cohen S. Bioengineered cardiac grafts: A new approach to

repair the infarcted myocardium? Circulation 2000;102(19 Suppl 3):III56-61.

12. Kellar RS, Shepherd BR, Larson DF, Naughton GK, Williams SK. Cardiac patch constructed from human fibroblasts attenuates reduction in cardiac function after acute infarct. Tissue Eng 2005;11(11-12):1678-87.

13. Krupnick AS, Kreisel D, Engels FH, Szeto WY, Plappert T, Popma SH, Flake AW, Rosengard BR. A novel small animal model of left ventricular tissue engineering. J Heart Lung Transplant 2002;21(2):233-43.

14. Robinson KA, Li J, Mathison M, Redkar A, Cui J, Chronos NA, Matheny RG, Badylak SF. Extracellular matrix scaffold for cardiac repair. Circulation 2005;112(9 Suppl):I135-43.

15. Zimmermann WH, Didié M, Wasmeier GH, Nixdorff U, Hess A, Melnychenko I, Boy O, Neuhuber WL, Weyand M, Eschenhagen T. Cardiac grafting of engineered heart tissue in syngenic rats. Circulation 2002;106(12 Suppl 1):I151-7.

16. Zimmermann WH, Melnychenko I, Wasmeier G, Didié M, Naito H, Nixdorff U, Hess A, Budinsky L, Brune K, Michaelis B and others. Engineered heart tissue grafts improve systolic and diastolic function in infarcted rat hearts. Nat Med 2006;12(4):452-8.

17. Callegari A, Bollini S, Iop L, Chiavegato A, Torregrossa G, Pozzobon M, Gerosa G, De Coppi P, Elvassore N, Sartore S. Neovascularization induced by porous collagen scaffold implanted on intact and cryoinjured rat hearts. Biomaterials 2007;28(36):5449-61.

18. Chachques JC, Trainini JC, Lago N, Cortes-Morichetti M, Schussler O, Carpentier A. Myocardial Assistance by Grafting a New Bioartificial Upgraded Myocardium (MAGNUM trial): clinical feasibility study. Ann Thorac Surg 2008;85(3):901-8.

19. Pozzobon M, Bollini S, Iop L, De Gaspari P, Chiavegato A, Rossi CA, Giuliani S, Fascetti Leon F, Elvassore N, Sartore S and others. Human bone marrow-derived CD133(+) cells delivered to a collagen patch on cryoinjured rat heart promote angiogenesis and arteriogenesis. Cell transplantation 2010;19(10):1247-60.

20. Simpson D, Liu H, Fan TM, Nerem R, Dudley SC. A tissue engineering approach to progenitor cell delivery results in significant cell engraftment and improved myocardial remodeling. Stem Cells 2007;25(9):2350-7.

21.   Dvir T, Kedem A, Ruvinov E, Levy O, Freeman I, Landa N, Holbova R, Feinberg MS, Dror S, Etzion Y and others. Prevascularization of cardiac patch on the omentum improves its therapeutic outcome. Proc Natl Acad Sci USA 2009;106(35):14990-5.

22.   Fujita M, Ishihara M, Morimoto Y, Simizu M, Saito Y, Yura H, Matsui T, Takase B, Hattori H, Kanatani Y and others. Efficacy of photocrosslinkable chitosan hydrogel containing fibroblast growth factor-2 in a rabbit model of chronic myocardial infarction. J Surg Res. Volume 126; 2005. p 27-33.

23.   Xiong Q, Hill KL, Li Q, Suntharalingam P, Mansoor A, Wang X, Jameel MN, Zhang P, Swingen C, Kaufman DS and others. A fibrin patch-based enhanced delivery of human embryonic stem cell-derived vascular cell transplantation in a porcine model of postinfarction left ventricular remodeling. Stem Cells 2011;29(2):367-75.

24.   Siepe M, Giraud M, Liljensten E, Nydegger U, Menasche P, Carrel T, Tevaearai HT. Construction of skeletal myoblast-based polyurethane scaffolds for myocardial repair. Artif Organs. Volume 31; 2007. p 425-433.

25.   Siepe M, Giraud MN, Pavlovic M, Receputo C, Beyersdorf F, Menasché P, Carrel T, Tevaearai HT. Myoblast-seeded biodegradable scaffolds to prevent post-myocardial infarction evolution toward heart failure. The Journal of Thoracic and Cardiovascular Surgery 2006;132(1):124-31.

26.   Fujimoto KL, Tobita K, Merryman WD, Guan J, Momoi N, Stolz DB, Sacks MS, Keller BB, Wagner WR. An elastic, biodegradable cardiac patch induces contractile smooth muscle and improves cardiac remodeling and function in subacute myocardial infarction. J Am Coll Cardiol. Volume 49; 2007. p 2292-2300.

27.   Piao H, Kwon J, Piao S, Sohn J, Lee Y, Bae J, Hwang KK, Kim D, Jeon O, Kim BS and others. Effects of cardiac patches engineered with bone marrow-derived mononuclear cells and PGCL scaffolds in a rat myocardial infarction model. Biomaterials. Volume 28; 2007. p 641-649.

28.   Jin J, Jeong SI, Shin YM, Lim KS, Shin H, Lee YM, Koh HC, Kim KS. Transplantation of mesenchymal stem cells within a poly(lactide-co-epsilon-caprolactone) scaffold improves cardiac function in a rat myocardial infarction model. Eur J Heart Fail 2009;11(2):147-53.

29.   Godier-Furnémont AF, Martens TP, Koeckert MS, Wan L, Parks J, Arai K, Zhang G, Hudson B, Homma S, Vunjak-Novakovic G. Composite

scaffold provides a cell delivery platform for cardiovascular repair. Proc Natl Acad Sci USA 2011;108(19):7974-9.

30. Tan MY, Zhi W, Wei RQ, Huang YC, Zhou KP, Tan B, Deng L, Luo JC, Li XQ, Xie HQ and others. Repair of infarcted myocardium using mesenchymal stem cell seeded small intestinal submucosa in rabbits. Biomaterials. Volume 30; 2009. p 3234-3240.

31. Wei H, Chen C, Lee W, Chiu I, Hwang S, Lin W, Huang CC, Yeh Y, Chang Y, Sung H. Bioengineered cardiac patch constructed from multilayered mesenchymal stem cells for myocardial repair. Biomaterials 2008;29(26):3547-56.

32. Zhang G, Hu Q, Braunlin EA, Suggs LJ, Zhang J. Enhancing efficacy of stem cell transplantation to the heart with a PEGylated fibrin biomatrix. Tissue Eng Pt A 2008;14(6):1025-36.

33. Nakamuta JS, Danoviz ME, Marques FLN, dos Santos L, Becker C, Goncalves GA, Vassallo PF, Schettert IT, Tucci PJF, Krieger JE. Cell Therapy Attenuates Cardiac Dysfunction Post Myocardial Infarction: Effect of Timing, Routes of Injection and a Fibrin Scaffold. PLoS ONE. Volume 4; 2009. p e6005.

34. Danoviz ME, Nakamuta JS, Marques FLN, dos Santos L, Alvarenga EC, dos Santos AA, Antonio EL, Schettert IT, Tucci PJ, Krieger JE. Rat Adipose Tissue-Derived Stem Cells Transplantation Attenuates Cardiac Dysfunction Post Infarction and Biopolymers Enhance Cell Retention. PLoS ONE. Volume 5; 2010. p e12077.

35. Guo HD, Wang HJ, Tan YZ, Wu JH. Transplantation of marrow-derived cardiac stem cells carried in fibrin improves cardiac function after myocardial infarction. Tissue Eng Pt A 2011;17(1-2):45-58.

36. Zhang X, Wang H, Ma X, Adila A, Wang B, Liu F, Chen B, Wang C, Ma Y. Preservation of the cardiac function in infarcted rat hearts by the transplantation of adipose-derived stem cells with injectable fibrin scaffolds. Exp Biol Med (Maywood) 2010;235(12):1505-15.

37. Yang HS, Bhang SH, Kim IK, Lee TJ, Kang JM, Lee DH, Lee SH, Hwang KC, Kim BS. In Situ Cardiomyogenic Differentiation of Implanted Bone Marrow Mononuclear Cells by Local Delivery of Transforming Growth Factor-β1. Cell transplantation 2011.

38. Nie SP, Wang X, Qiao SB, Zeng QT, Jiang JQ, Liu XQ, Zhu XM, Cao GX, Ma CS. Improved myocardial perfusion and cardiac function by

controlled-release basic fibroblast growth factor using fibrin glue in a canine infarct model. J Zhejiang Univ Sci B 2010;11(12):895-904.

39. Yu J, Gu Y, Du KT, Mihardja S, Sievers RE, Lee RJ. The effect of injected RGD modified alginate on angiogenesis and left ventricular function in a chronic rat infarct model. Biomaterials 2009;30(5):751-6.

40. Ruvinov E, Leor J, Cohen S. The promotion of myocardial repair by the sequential delivery of IGF-1 and HGF from an injectable alginate biomaterial in a model of acute myocardial infarction. Biomaterials. Volume 32; 2011. p 565-578.

41. Hao X, Silva EA, Månsson-Broberg A, Grinnemo KH, Siddiqui AJ, Dellgren G, Wärdell E, Brodin LA, Mooney DJ, Sylvén C. Angiogenic effects of sequential release of VEGF-A165 and PDGF-BB with alginate hydrogels after myocardial infarction. Cardiovasc Res 2007;75(1):178-85.

42. Yu J, Du KT, Fang Q, Gu Y, Mihardja SS, Sievers RE, Wu JC, Lee RJ. The use of human mesenchymal stem cells encapsulated in RGD modified alginate microspheres in the repair of myocardial infarction in the rat. Biomaterials. Volume 31; 2010. p 7012-7020.

43. Tsur-Gang O, Ruvinov E, Landa N, Holbova R, Feinberg MS, Leor J, Cohen S. The effects of peptide-based modification of alginate on left ventricular remodeling and function after myocardial infarction. Biomaterials. Volume 30; 2009. p 189-195.

44. Landa N, Miller L, Feinberg MS, Holbova R, Shachar M, Freeman I, Cohen S, Leor J. Effect of injectable alginate implant on cardiac remodeling and function after recent and old infarcts in rat. Circulation 2008;117(11):1388-96.

45. Mihardja SS, Sievers RE, Lee RJ. The effect of polypyrrole on arteriogenesis in an acute rat infarct model. Biomaterials 2008;29(31):4205-10.

46. BioLineRx L. Safety and Feasibility of the Injectable BL-1040 Implant. Clinical Trials.gov NCT00557531. 2007.

47. Mukherjee R, Zavadzkas JA, Saunders SM, McLean JE, Jeffords LB, Beck C, Stroud RE, Leone AM, Koval CN, Rivers WT and others. Targeted myocardial microinjections of a biocomposite material reduces infarct expansion in pigs. Ann Thorac Surg. Volume 86; 2008. p 1268-1277.

48. Lu WN, Lü SH, Wang HB, Li DX, Duan CM, Liu ZQ, Hao T, He WJ, Xu B, Fu Q and others. Functional improvement of infarcted heart by co-injection of embryonic stem cells with temperature-responsive chitosan hydrogel. Tissue Eng Pt A 2009;15(6):1437-47.

49. Lue S, Wang H, Lu W, Liu S, Lin Q, Li D, Duan C, Hao T, Zhou J, Wang Y and others. Both the Transplantation of Somatic Cell Nuclear Transfer- and Fertilization-Derived Mouse Embryonic Stem Cells with Temperature-Responsive Chitosan Hydrogel Improve Myocardial Performance in Infarcted Rat Hearts. Tissue Eng Pt A. Volume 16; 2010. p 1303-1315.

50. Wang H, Zhang X, Li Y, Ma Y, Zhang Y, Liu Z, Zhou J, Lin Q, Wang Y, Duan C and others. Improved myocardial performance in infarcted rat heart by co-injection of basic fibroblast growth factor with temperature-responsive Chitosan hydrogel. J Heart Lung Transpl. Volume 29; 2010. p 881-887.

51. Shao ZQ, Takaji K, Katayama Y, Kunitomo R, Sakaguchi H, Lai ZF, Kawasuji M. Effects of intramyocardial administration of slow-release basic fibroblast growth factor on angiogenesis and ventricular remodeling in a rat infarct model. Circ J. Volume 70; 2006. p 471-477.

52. Liu Y, Sun L, Huan Y, Zhao H, Deng J. Effects of basic fibroblast growth factor microspheres on angiogenesis in ischemic myocardium and cardiac function: analysis with dobutamine cardiovascular magnetic resonance tagging. Eur J Cardio-Thorac. Volume 30; 2006. p 103-107.

53. Huang NF, Yu J, Sievers R, Li S, Lee RJ. Injectable biopolymers enhance angiogenesis after myocardial infarction. Tissue Eng 2005;11(11-12):1860-6.

54. Thompson CA, Nasseri BA, Makower J, Houser S, McGarry M, Lamson T, Pomerantseva I, Chang JY, Gold HK, Vacanti JP and others. Percutaneous transvenous cellular cardiomyoplasty. A novel nonsurgical approach for myocardial cell transplantation. J Am Coll Cardiol 2003;41(11):1964-71.

55. Dai W, Wold LE, Dow JS, Kloner RA. Thickening of the infarcted wall by collagen injection improves left ventricular function in rats: a novel approach to preserve cardiac function after myocardial infarction. J Am Coll Cardiol 2005;46(4):714-9.

56. Ou L, Li W, Zhang Y, Wang W, Liu J, Sorg H, Furlani D, Gäbel R, Mark P, Klopsch C and others. Intracardiac injection of matrigel induces stem

cell recruitment and improves cardiac functions in a rat myocardial infarction model. J Cell Mol Med 2011;15(6):1310-8.

57. Laflamme MA, Chen KY, Naumova AV, Muskheli V, Fugate JA, Dupras SK, Reinecke H, Xu C, Hassanipour M, Police S and others. Cardiomyocytes derived from human embryonic stem cells in pro-survival factors enhance function of infarcted rat hearts. Nat Biotechnol 2007;25(9):1015-24.

58. Zhang PC, Zhang H, Wang H, Wei YJ, Hu SS. Artificial matrix helps neonatal cardiomyocytes restore injured myocardium in rats. Artif Organs. Volume 30; 2006. p 86-93.

59. Okada M, Payne TR, Oshima H, Momoi N, Tobita K, Huard J. Differential efficacy of gels derived from small intestinal submucosa as an injectable biomaterial for myocardial infarct repair. Biomaterials. Volume 31; 2010. p 7678-7683.

60. Zhao ZQ, Puskas JD, Xu D, Wang NP, Mosunjac M, Guyton RA, Vinten-Johansen J, Matheny R. Improvement in cardiac function with small intestine extracellular matrix is associated with recruitment of C-kit cells, myofibroblasts, and macrophages after myocardial infarction. J Am Coll Cardiol 2010;55(12):1250-61.

61. Singelyn JM, DeQuach JA, Seif-Naraghi SB, Littlefield RB, Schup-Magoffin PJ, Christman KL. Naturally derived myocardial matrix as an injectable scaffold for cardiac tissue engineering. Biomaterials. Volume 30; 2009. p 5409-5416.

62. Seif-Naraghi SB, Salvatore MA, Schup-Magoffin PJ, Hu DP, Christman KL. Design and Characterization of an Injectable Pericardial Matrix Gel: A Potentially Autologous Scaffold for Cardiac Tissue Engineering. Tissue Eng Pt A. Volume 16; 2010. p 2017-2027.

63. Yoon SJ, Fang YH, Lim CH, Kim BS, Son HS, Park Y, Sun K. Regeneration of Ischemic Heart Using Hyaluronic Acid-Based Injectable Hydrogel. J Biomed Mater Res B. Volume 91B; 2009. p 163-171.

64. Ifkovits JL, Tous E, Minakawa M, Morita M, Robb JD, Koomalsingh KJ, Gorman JH, Gorman RC, Burdick JA. Injectable hydrogel properties influence infarct expansion and extent of postinfarction left ventricular remodeling in an ovine model. Proc Natl Acad Sci USA 2010;107(25):11507-12.

65. Dubois G, Segers VF, Bellamy V, Sabbah L, Peyrard S, Bruneval P, Hagège AA, Lee RT, Menasché P. Self-assembling peptide nanofibers and

skeletal myoblast transplantation in infarcted myocardium. J Biomed Mater Res Part B Appl Biomater 2008;87(1):222-8.

66.   Lin Y, Yeh M, Yang Y, Tsai D, Chu T, Shih Y, Chang M, Liu Y, Tang AC, Chen T and others. Intramyocardial peptide nanofiber injection improves postinfarction ventricular remodeling and efficacy of bone marrow cell therapy in pigs. Circulation 2010;122(11 Suppl):S132-41.

67.   Kim JH, Jung Y, Kim SH, Sun K, Choi J, Kim HC, Park Y, Kim SH. The enhancement of mature vessel formation and cardiac function in infarcted hearts using dual growth factor delivery with self-assembling peptides. Biomaterials 2011;32(26):6080-8.

68.   Davis ME, Hsieh PCH, Takahashi T, Song Q, Zhang SG, Kamm RD, Grodzinsky AJ, Anversa P, Lee RT. Local myocardial insulin-like growth factor 1 (IGF-1) delivery with biotinylated peptide nanofibers improves cell therapy for myocardial infarction. Proc Natl Acad Sci USA. Volume 103; 2006. p 8155-8160.

69.   Ryan LP, Matsuzaki K, Noma M, Jackson BM, Eperjesi TJ, Plappert TJ, John-Sutton MGS, Gorman JH, Gorman RC. Dermal Filler Injection: A Novel Approach for Limiting Infarct Expansion. Ann Thorac Surg. Volume 87; 2009. p 148-155.

70.   Morita M, Eckert CE, Matsuzaki K, Noma M, Ryan LP, Burdick JA, Jackson BM, Gorman JH, Sacks MS, Gorman RC. Modification of infarct material properties limits adverse ventricular remodeling. Ann Thorac Surg 2011;92(2):617-24.

71.   Dobner S, Bezuidenhout D, Govender P, Zilla P, Davies N. A synthetic non-degradable polyethylene glycol hydrogel retards adverse post-infarct left ventricular remodeling. J Card Fail 2009;15(7):629-36.

72.   Rane AA, Chuang JS, Shah A, Hu DP, Dalton ND, Gu Y, Peterson KL, Omens JH, Christman KL. Increased Infarct Wall Thickness by a Bio-Inert Material Is Insufficient to Prevent Negative Left Ventricular Remodeling after Myocardial Infarction. PLoS ONE. Volume 6; 2011. p e21571.

73.   Kraehenbuehl TP, Ferreira LS, Hayward AM, Nahrendorf M, van der Vlies AJ, Vasile E, Weissleder R, Langer R, Hubbell JA. Human embryonic stem cell-derived microvascular grafts for cardiac tissue preservation after myocardial infarction. Biomaterials. Volume 32; 2011. p 1102-1109.

74. Wu J, Zeng F, Huang X, Chung JC, Konecny F, Weisel RD, Li R. Infarct stabilization and cardiac repair with a VEGF-conjugated, injectable hydrogel. Biomaterials. Volume 32; 2011. p 579-586.

75. Jiang XJ, Wang T, Li XY, Wu DQ, Zheng ZB, Zhang JF, Chen JL, Peng B, Jiang H, Huang C and others. Injection of a novel synthetic hydrogel preserves left ventricle function after myocardial infarction. Journal of biomedical materials research Part A 2009;90(2):472-7.

76. Wang T, Jiang XJ, Tang Q, Li XY, Lin T, Wu DQ, Zhang XZ, Okello E. Bone marrow stem cells implantation with alpha-cyclodextrin/MPEG-PCL-MPEG hydrogel improves cardiac function after myocardial infarction. Acta biomaterialia. Volume 5; 2009. p 2939-2944.

77. Wang T, Jiang XJ, Lin T, Ren S, Li XY, Zhang XZ, Tang Q. The inhibition of postinfarct ventricle remodeling without polycythaemia following local sustained intramyocardial delivery of erythropoietin within a supramolecular hydrogel. Biomaterials. Volume 30; 2009. p 4161-4167.

78. Wang T, Wu DQ, Jiang XJ, Zhang XZ, Li XY, Zhang JF, Zheng ZB, Zhuo R, Jiang H, Huang C. Novel thermosensitive hydrogel injection inhibits post-infarct ventricle remodelling. Eur J Heart Fail 2009;11(1):14-9.

79. Garbern JC, Minami E, Stayton PS, Murry CE. Delivery of basic fibroblast growth factor with a pH-responsive, injectable hydrogel to improve angiogenesis in infarcted myocardium. Biomaterials 2011;32(9):2407-16.

80. Fujimoto KL, Ma Z, Nelson DM, Hashizume R, Guan J, Tobita K, Wagner WR. Synthesis, characterization and therapeutic efficacy of a biodegradable, thermoresponsive hydrogel designed for application in chronic infarcted myocardium. Biomaterials 2009;30(26):4357-68.

81. Li XY, Wang T, Jiang XJ, Lin T, Wu DQ, Zhang XZ, Okello E, Xu H, Yuan M. Injectable Hydrogel Helps Bone Marrow-Derived Mononuclear Cells Restore Infarcted Myocardium. Cardiology. Volume 115; 2010. p 194-199.

82. Wall ST, Yeh CC, Tu RY, Mann MJ, Healy KE. Biomimetic matrices for myocardial stabilization and stem cell transplantation. Journal of biomedical materials research Part A 2010;95(4):1055-66.

83. Sarig U, Machluf M. Engineering cell platforms for myocardial regeneration. Expert Opin Biol Ther 2011;11(8):1055-77.

84. Hamdi H, Furuta A, Bellamy V, Bel A, Puymirat E, Peyrard S, Agbulut O, Menasché P. Cell delivery: intramyocardial injections or epicardial deposition? A head-to-head comparison. Ann Thorac Surg 2009;87(4):1196-203.

85. Giraud MN, Ayuni E, Cook S, Siepe M, Carrel TP, Tevaearai HT. Hydrogel-based engineered skeletal muscle grafts normalize heart function early after myocardial infarction. Artif Organs 2008;32(9):692-700.

86. Ott HC, Matthiesen TS, Goh SK, Black LD, Kren SM, Netoff TI, Taylor DA. Perfusion-decellularized matrix: using nature's platform to engineer a bioartificial heart. Nat Med 2008;14(2):213-21.

87. Giraud MN, Flueckiger R, Cook S, Ayuni E, Siepe M, Carrel T, Tevaearai H. Long-term evaluation of myoblast seeded patches implanted on infarcted rat hearts. Artif Organs 2010;34(6):E184-92.

88. Singelyn JM, Christman KL. Injectable Materials for the Treatment of Myocardial Infarction and Heart Failure: The Promise of Decellularized Matrices. Journal of cardiovascular translational research 2010.

89. Christman KL, Singelyn JM, Salvatore M, Schup-Magoffin PJ, Hu DP, Johnson T, Bartels K, DeMaria AN, Dib N. Catheter-Deliverable Hydrogel Derived from Decellularized Ventricular Extracellular Matrix Increases Cardiomyocyte Survival and Preserves Cardiac Function Post-Myocardial Infarction. Journal of the American College of Cardiology 2011;57(14):E2017-E2017.

90. Leor J, Tuvia S, Guetta V, Manczur F, Castel D, Willenz U, Petnehazy O, Landa N, Feinberg MS, Konen E and others. Intracoronary injection of in situ forming alginate hydrogel reverses left ventricular remodeling after myocardial infarction in Swine. Journal of the American College of Cardiology 2009;54(11):1014-23.

91. Christman KL, Fok HH, Sievers RE, Fang Q, Lee RJ. Fibrin glue alone and skeletal myoblasts in a fibrin scaffold preserve cardiac function after myocardial infarction. Tissue engineering 2004;10(3-4):403-9.

92. Christman KL, Vardanian AJ, Fang Q, Sievers RE, Fok HH, Lee RJ. Injectable fibrin scaffold improves cell transplant survival, reduces infarct expansion, and induces neovasculature formation in ischemic myocardium. J Am Coll Cardiol 2004;44(3):654-60.

93. Leor J, Amsalem Y, Cohen S. Cells, scaffolds, and molecules for myocardial tissue engineering. Pharmacol Ther 2005;105(2):151-63.

94.   Lutolf MP, Hubbell JA. Synthetic biomaterials as instructive extracellular microenvironments for morphogenesis in tissue engineering. Nat Biotechnol 2005;23(1):47-55.

95.   Seif-Naraghi SB, Horn D, Schup-Magoffin PA, Madani MM, Christman KL. Patient-to-Patient Variability in Autologous Pericardial Matrix Scaffolds for Cardiac Repair. Journal of cardiovascular translational research 2011;4(5):545-56.

96.   Wall ST, Walker JC, Healy KE, Ratcliffe MB, Guccione JM. Theoretical impact of the injection of material into the myocardium: a finite element model simulation. Circulation 2006;114(24):2627-35.

97.   Herpel E, Pritsch M, Koch A, Dengler TJ, Schirmacher P, Schnabel PA. Interstitial fibrosis in the heart: differences in extracellular matrix proteins and matrix metalloproteinases in end-stage dilated, ischaemic and valvular cardiomyopathy. Histopathology 2006;48(6):736-47.

98.   Gepstein L, Ding C, Rehemedula D, Wilson EE, Yankelson L, Caspi O, Gepstein A, Huber I, Olgin JE. In vivo assessment of the electrophysiological integration and arrhythmogenic risk of myocardial cell transplantation strategies. Stem Cells 2010;28(12):2151-61.

99.   Lloyd-Jones. Heart Disease and Stroke Statistics-2010 Update: A Report From the American Heart Association (vol 121, pg e46, 2010). Circulation 2010;121(12):E260-E260.

100.   Christman KL, Fok HH, Sievers RE, Fang Q, Lee RJ. Fibrin glue alone and skeletal myoblasts in a fibrin scaffold preserve cardiac function after myocardial infarction. Tissue Eng 2004;10(3-4):403-9.

101.   Jackson BM, Gorman JH, Salgo IS, Moainie SL, Plappert T, St John-Sutton M, Edmunds LH, Gorman RC. Border zone geometry increases wall stress after myocardial infarction: contrast echocardiographic assessment. Am J Physiol Heart Circ Physiol 2003;284(2):H475-9.

102.   Davis ME, Motion JP, Narmoneva DA, Takahashi T, Hakuno D, Kamm RD, Zhang S, Lee RT. Injectable self-assembling peptide nanofibers create intramyocardial microenvironments for endothelial cells. Circulation 2005;111(4):442-50.

103.   Singelyn JM, DeQuach JA, Seif-Naraghi SB, Littlefield RB, Schup-Magoffin PJ, Christman KL. Naturally derived myocardial matrix as an injectable scaffold for cardiac tissue engineering. Biomaterials 2009;30(29):5409-16.

104. Singelyn JM, Christman KL. Injectable Materials for the Treatment of Myocardial Infarction and Heart Failure: The Promise of Decellularized Matrices. Journal of cardiovascular translational research 2010;3:478–486.

105. Nelson DM, Ma Z, Fujimoto KL, Hashizume R, Wagner WR. Intra-myocardial biomaterial injection therapy in the treatment of heart failure: Materials, outcomes and challenges. Acta biomaterialia. Volume 7; 2011. p 1-15.

106. Harris JM. Introduction to Biotechnical and Biomedical Applications of Poly (Ethylene Glycol) In: Harris JM, editor. Poly (Ethylene Glycol) Chemistry. New York & London: Plenum Press; 1992. p 3.

107. Lin-Gibson S, Bencherif S, Cooper JA, Wetzel SJ, Antonucci JM, Vogel BM, Horkay F, Washburn NR. Synthesis and characterization of PEG dimethacrylates and their hydrogels. Biomacromolecules. Volume 5; 2004. p 1280-1287.

108. Uhrich KE, Cannizzaro SM, Langer RS, Shakesheff KM. Polymeric systems for controlled drug release. Chem Rev. Volume 99; 1999. p 3181-3198.

109. Ali Khademhosseini JB, Mehmet Toner, Shuichi Takayama. Micro- and Nanoengineering of the Cell Microenvironment, Technologies and Applications (Engineering in Medicine & Biology). . Boston and London Artech House; 2008.

110. Chandrashekhar P. Pathak ASS, Peter G., Edelman; Incept, LLC, Lexington, MA, assignee. Biocompatible Crosslinked Polymers. US patent US 6,566,406 BI. 2003 May 20 2003.

111. Lutolf MP, Hubbell JA. Synthesis and physicochemical characterization of end-linked poly(ethylene glycol)-co-peptide hydrogels formed by Michael-type addition. Biomacromolecules 2003;4(3):713-22.

112. Anumolu SS, DeSantis AS, Menjoge AR, Hahn RA, Beloni JA, Gordon MK, Sinko PJ. Doxycycline loaded poly(ethylene glycol) hydrogels for healing vesicant-induced ocular wounds. Biomaterials 2010;31(5):964-74.

113. Iwanaga Y, Hoshijima M, Gu Y, Iwatate M, Dieterle T, Ikeda Y, Date MO, Chrast J, Matsuzaki M, Peterson KL and others. Chronic phospholamban inhibition prevents progressive cardiac dysfunction and pathological remodeling after infarction in rats. J Clin Invest 2004;113(5):727-36.

114. Chuang JS, Zemljic-Harpf A, Ross RS, Frank LR, McCulloch AD, Omens JH. Determination of three-dimensional ventricular strain distributions in gene-targeted mice using tagged MRI. Magn Reson Med 2010;64(5):1281-8.

115. Wang L, Deng J, Tian W, Xiang B, Yang T, Li G, Wang J, Gruwel M, Kashour T, Rendell J and others. Adipose-derived stem cells are an effective cell candidate for treatment of heart failure: an MR imaging study of rat hearts. Am J Physiol-Heart C. Volume 297; 2009. p H1020-H1031.

116. Axel L, Dougherty L. MR imaging of motion with spatial modulation of magnetization. Radiology 1989;171(3):841-5.

117. Osman NF, Kerwin WS, McVeigh ER, Prince JL. Cardiac motion tracking using CINE harmonic phase (HARP) magnetic resonance imaging. Magn Reson Med 1999;42(6):1048-60.

118. Allman AJ, McPherson TB, Badylak SF, Merrill LC, Kallakury B, Sheehan C, Raeder RH, Metzger DW. Xenogeneic extracellular matrix grafts elicit a Th2-restricted immune response. Transplantation. Volume 71; 2001. p 1631-1640.

119. Badylak S, Kokini K, Tullius B, Simmons-Byrd A, Morff R. Morphologic study of small intestinal submucosa as a body wall repair device. J Surg Res. Volume 103; 2002. p 190-202.

120. Valentin JE, Badylak JS, McCabe GP, Badylak SF. Extracellular matrix bioscaffolds for orthopaedic applications - A comparative histologic study. J Bone Joint Surg Am. Volume 88A; 2006. p 2673-2686.

121. Badylak SF, Valentin JE, Ravindra AK, McCabe GP, Stewart-Akers AM. Macrophage phenotype as a determinant of biologic scaffold remodeling. Tissue Eng Pt A 2008;14(11):1835-42.

122. Pfeffer JM, Pfeffer MA, Fletcher PJ, Braunwald E. Progressive ventricular remodeling in rat with myocardial infarction. Am J Physiol 1991;260(5 Pt 2):H1406-14.

123. Draget KI, Stokke BT, Yuguchi Y, Urakawa H, Kajiwara K. Small-angle X-ray scattering and rheological characterization of alginate gels. 3. Alginic acid gels. Biomacromolecules 2003;4(6):1661-8.

124. Wu DQ, Qiu F, Wang T, Jiang XJ, Zhang XZ, Zhuo RX. Toward the development of partially biodegradable and injectable thermoresponsive

hydrogels for potential biomedical applications. ACS Appl Mater Interfaces 2009;1(2):319-27.

125. Rizzi SC, Hubbell JA. Recombinant protein-co-PEG networks as cell-adhesive and proteolytically degradable hydrogel matrixes. Part I: Development and physicochemical characteristics. Biomacromolecules 2005;6(3):1226-38.

126. Berry MF, Engler AJ, Woo YJ, Pirolli TJ, Bish LT, Jayasankar V, Morine KJ, Gardner TJ, Discher DE, Sweeney HL. Mesenchymal stem cell injection after myocardial infarction improves myocardial compliance. Am J Physiol Heart Circ Physiol 2006;290(6):H2196-203.

127. Thompson WD, Smith EB, Stirk CM, Marshall FI, Stout AJ, Kocchar A. Angiogenic activity of fibrin degradation products is located in fibrin fragment E. J Pathol 1992;168(1):47-53.

128. Mihardja SS, Gao DW, Sievers RE, Fang QZ, Feng JJ, Wang JM, Vanbrocklin HF, Larrick JW, Huang M, Dae M and others. Targeted In Vivo Extracellular Matrix Formation Promotes Neovascularization in a Rodent Model of Myocardial Infarction. Plos One 2010;5(4):-.

129. Nam JO, Kim JE, Jeong HW, Lee SJ, Lee BH, Choi JY, Park RW, Park JY, Kim IS. Identification of the alphavbeta3 integrin-interacting motif of betaig-h3 and its anti-angiogenic effect. J Biol Chem 2003;278(28):25902-9.

130. Jugdutt BI. Ventricular remodeling after infarction and the extracellular collagen matrix: when is enough enough? Circulation 2003;108(11):1395-403.

131. Vick GW. The gold standard for noninvasive imaging in coronary heart disease: magnetic resonance imaging. Curr Opin Cardiol 2009;24(6):567-79.

132. Karamitsos TD, Francis JM, Myerson S, Selvanayagam JB, Neubauer S. The role of cardiovascular magnetic resonance imaging in heart failure. J Am Coll Cardiol 2009;54(15):1407-24.

133. Blom AS, Mukherjee R, Pilla JJ, Lowry AS, Yarbrough WM, Mingoia JT, Hendrick JW, Stroud RE, McLean JE, Affuso J and others. Cardiac support device modifies left ventricular geometry and myocardial structure after myocardial infarction. Circulation 2005;112(9):1274-83.

134. Hsieh PC, Davis ME, Gannon J, MacGillivray C, Lee RT. Controlled delivery of PDGF-BB for myocardial protection using injectable self-assembling peptide nanofibers. J Clin Invest 2006;116(1):237-48.

135. Ryu JH, Kim IK, Cho SW, Cho MC, Hwang KK, Piao H, Piao S, Lim SH, Hong YS, Choi CY and others. Implantation of bone marrow mononuclear cells using injectable fibrin matrix enhances neovascularization in infarcted myocardium. Biomaterials 2005;26(3):319-26.

136. Kong HJ, Lee KY, Mooney DJ. Decoupling the dependence of rheological/mechanical properties of hydrogels from solids concentration. Polymer. Volume 43; 2002. p 6239-+.

137. Sierra DH, Eberhardt AW, Lemons JE. Failure characteristics of multiple-component fibrin-based adhesives. J Biomed Mater Res. Volume 59; 2002. p 1-11.

138. Ikaria Holdings I. IK-500 for the Prevention of Remodeling of the Ventricle and Congestive Heart Failure After Acute Myocardial Infarction (PRESERVATION I) ClinicalTrials.gov NCT01226563.

139. Lutolf MP, Weber FE, Schmoekel HG, Schense JC, Kohler T, Müller R, Hubbell JA. Repair of bone defects using synthetic mimetics of collagenous extracellular matrices. Nat Biotechnol 2003;21(5):513-8.

140. Michel R, Pasche S, Textor M, Castner DG. Influence of PEG architecture on protein adsorption and conformation. Langmuir 2005;21(26):12327-32.

141. Gnecchi M, Zhang Z, Ni A, Dzau VJ. Paracrine mechanisms in adult stem cell signaling and therapy. Circulation Research 2008;103(11):1204-19.

142. Laflamme MA, Zbinden S, Epstein SE, Murry CE. Cell-based therapy for myocardial ischemia and infarction: pathophysiological mechanisms. Annu Rev Pathol 2007;2:307-39.

143. Mirotsou M, Jayawardena TM, Schmeckpeper J, Gnecchi M, Dzau VJ. Paracrine mechanisms of stem cell reparative and regenerative actions in the heart. Journal of Molecular and Cellular Cardiology 2011;50(2):280-9.

144. Ruvinov E, Harel-Adar T, Cohen S. Bioengineering the Infarcted Heart by Applying Bio-inspired Materials. Journal of cardiovascular translational research 2011.

145. Tous E, Purcell B, Ifkovits JL, Burdick JA. Injectable Acellular Hydrogels for Cardiac Repair. Journal of cardiovascular translational research 2011.

146. Badylak SF, Gilbert TW. Immune response to biologic scaffold materials. Semin Immunol 2008;20(2):109-16.

147. Brown BN, Londono R, Tottey S, Zhang L, Kukla KA, Wolf MT, Daly KA, Reing JE, Badylak SF. Macrophage phenotype as a predictor of constructive remodeling following the implantation of biologically derived surgical mesh materials. Acta biomaterialia 2012;8(3):978-87.

148. Sicari BM, Johnson SA, Siu BF, Crapo PM, Daly KA, Jiang H, Medberry CJ, Tottey S, Turner NJ, Badylak SF. The effect of source animal age upon the in vivo remodeling characteristics of an extracellular matrix scaffold. Biomaterials 2012;33(22):5524-33.

149. Brown BN, Valentin JE, Stewart-Akers AM, McCabe GP, Badylak SF. Macrophage phenotype and remodeling outcomes in response to biologic scaffolds with and without a cellular component. Biomaterials 2009;30(8):1482-91.

150. Sica A, Mantovani A. Macrophage plasticity and polarization: in vivo veritas. J Clin Invest 2012;122(3):787-95.

151. Kanellakis P, Ditiatkovski M, Kostolias G, Bobik A. A pro-fibrotic role for interleukin-4 in cardiac pressure overload. Cardiovasc Res 2012;95(1):77-85.

152. Yu J, Christman KL, Chin E, Sievers RE, Saeed M, Lee RJ. Restoration of left ventricular geometry and improvement of left ventricular function in a rodent model of chronic ischemic cardiomyopathy. J Thorac Cardiov Sur. Volume 137; 2009. p 180-187.

153. Hagège AA, Marolleau JP, Vilquin JT, Alhéritière A, Peyrard S, Duboc D, Abergel E, Messas E, Mousseaux E, Schwartz K and others. Skeletal myoblast transplantation in ischemic heart failure: long-term follow-up of the first phase I cohort of patients. Circulation 2006;114(1 Suppl):I108-13.

154. Dib N, Michler RE, Pagani FD, Wright S, Kereiakes DJ, Lengerich R, Binkley P, Buchele D, Anand I, Swingen C and others. Safety and feasibility of autologous myoblast transplantation in patients with ischemic cardiomyopathy: four-year follow-up. Circulation 2005;112(12):1748-55.

155. Siminiak T, Kalawski R, Fiszer D, Jerzykowska O, Rzeźniczak J, Rozwadowska N, Kurpisz M. Autologous skeletal myoblast transplantation for the treatment of postinfarction myocardial injury: phase I clinical study with 12 months of follow-up. Am Heart J 2004;148(3):531-7.

156. Efimov IR, Nikolski VP, Salama G. Optical imaging of the heart. Circulation Research 2004;95(1):21-33.

157. Mills WR, Mal N, Forudi F, Popovic ZB, Penn MS, Laurita KR. Optical mapping of late myocardial infarction in rats. Am J Physiol Heart Circ Physiol 2006;290(3):H1298-306.

158. Ding C, Gepstein L, Nguyen DT, Wilson E, Hulley G, Beaser A, Lee RJ, Olgin J. High-resolution optical mapping of ventricular tachycardia in rats with chronic myocardial infarction. Pacing Clin Electrophysiol 2010;33(6):687-95.

159. Costa AR, Panda NC, Yong S, Mayorga ME, Pawlowski GP, Fan K, Penn MS, Laurita KR. Optical mapping of cryoinjured rat myocardium grafted with mesenchymal stem cells. Am J Physiol Heart Circ Physiol 2012;302(1):H270-7.

160. Frechet JMJ, Broaders KE, Cohen JA, Beaudette TT, Bachelder EM. Acetalated dextran is a chemically and biologically tunable material for particulate immunotherapy. Proceedings of the National Academy of Sciences of the United States of America 2009;106(14):5497-5502.

161. Bachelder EM, Beaudette TT, Broaders KE, Dashe J, Frechet JM. Acetal-derivatized dextran: an acid-responsive biodegradable material for therapeutic applications. J Am Chem Soc 2008;130(32):10494-5.

162. Fedorov VV, Lozinsky IT, Sosunov EA, Anyukhovsky EP, Rosen MR, Balke CW, Efimov IR. Application of blebbistatin as an excitation-contraction uncoupler for electrophysiologic study of rat and rabbit hearts. Heart Rhythm 2007;4(5):619-26.

163. Sung D, JSJP C, Mills R, McCulloch AD. Phase shifting prior to spatial filtering enhances optical recordings of cardiac action potential propagation. Ann Biomed Eng 2001;29(10):854-61.

164. Sampson KJ, Henriquez CS. Electrotonic influences on action potential duration dispersion in small hearts: a simulation study. Am J Physiol Heart Circ Physiol 2005;289(1):H350-60.

165. Henriquez CS. Simulating the electrical behavior of cardiac tissue using the bidomain model. Crit Rev Biomed Eng 1993;21(1):1-77.

166. Roth BJ. How the anisotropy of the intracellular and extracellular conductivities influences stimulation of cardiac muscle. J Math Biol 1992;30(6):633-46.

167. Danik SB, Liu F, Zhang J, Suk HJ, Morley GE, Fishman GI, Gutstein DE. Modulation of cardiac gap junction expression and arrhythmic susceptibility. Circulation Research 2004;95(10):1035-41.

168. Menasché P. Stem cell therapy for heart failure: are arrhythmias a real safety concern? Circulation 2009;119(20):2735-40.

169. Wei HJ, Yang HH, Chen CH, Lin WW, Chen SC, Lai PH, Chang Y, Sung HW. Gelatin microspheres encapsulated with a nonpeptide angiogenic agent, ginsenoside Rg1, for intramyocardial injection in a rat model with infarcted myocardium. J Control Release 2007;120(1-2):27-34.

170. Seshadri G, Sy JC, Brown M, Dikalov S, Yang SC, Murthy N, Davis ME. The delivery of superoxide dismutase encapsulated in polyketal microparticles to rat myocardium and protection from myocardial ischemia-reperfusion injury. Biomaterials 2010;31(6):1372-9.

171. Sy JC, Seshadri G, Yang SC, Brown M, Oh T, Dikalov S, Murthy N, Davis ME. Sustained release of a p38 inhibitor from non-inflammatory microspheres inhibits cardiac dysfunction. Nat Mater 2008;7(11):863-8.

172. Roger VL, Go AS, Lloyd-Jones DM, Benjamin EJ, Berry JD, Borden WB, Bravata DM, Dai S, Ford ES, Fox CS and others. Heart disease and stroke statistics--2012 update: a report from the American Heart Association. Circulation 2012;125(1):e2-e220.

173. JM. H. Chemistry, Biotechnical and Biomedical Applications.: New York: Plenus Press; 1992.

174. Singelyn JM, Christman KL. Modulation of material properties of a decellularized myocardial matrix scaffold. Macromol Biosci 2011;11(6):731-8.